Effect of Carbon Dioxide on SAES® St909 Methane Cracking

by

J. E. Klein

Westinghouse Savannah River Company
Savannah River Site
Aiken, South Carolina 29808

DOE Contract No. **DE-AC09-96SR18500**

WSRC-TR-2002-00286

August 22, 2002

EFFECT OF CARBON DIOXIDE ON SAES ST909 METHANE CRACKING (U)

J. E. Klein

Savannah River Technology Center

SUMMARY

St909 can crack methane, carbon dioxide, and ammonia under a variety of operation conditions with efficiencies influenced greatly by other impurities in the gas stream and the carrier gas composition. The bench scale tests at the relatively high feed impurity levels of 5% demonstrated the impact of different parameters in relatively short duration tests.

The majority of tests were performed with a methane plus carbon dioxide feed composition of 5% at 700°C and 800°C for 27 hours: all at 760 torr pressure. Carrier gases included helium, helium with 2% ammonia, hydrogen, and nitrogen. In all cases, temperatures of 800°C gave higher methane and carbon dioxide cracking efficiencies than at 700°C, but this sometimes produced the undesirable result of releasing a higher concentration of carbon monoxide from the test bed.

Methane decomposition, or cracking, was most efficient in helium and less efficient in hydrogen or nitrogen. Hydrogen suppressed the driving force for methane decomposition while nitrogen absorption by the St909 interferes with methane decomposition. Methane cracking in the presence of ammonia is reduced by the nitrogen absorbed by the getter, not by the hydrogen released from ammonia decomposition.

Carbon dioxide decomposition was most efficient in hydrogen, followed by helium, then nitrogen. The high carbon dioxide cracking efficiency in hydrogen was due to methane formation and later, water formation by the getter. Carbon dioxide decomposition in nitrogen, as was found with methane, was reduced by nitrogen absorption by the getter interfering with the decomposition and diffusion processes.

Methane decomposition in the presence of carbon dioxide was reduced in all carrier gases due to the preference of St909 to decompose carbon dioxide over methane. The proposed mechanisms show carbon dioxide first decomposing to carbon monoxide which then decomposes preferentially over methane. In a helium carrier, methane decomposition can be stopped completely by carbon dioxide. In a hydrogen carrier, methane concentrations can be produced which exceed feed values; water can also be formed. In a nitrogen carrier, methane may be cracked, but at extremely low efficiencies.

Classification: Unclassified Technical Reviewer:

Authorized Derivative Classifier/Date

INTRODUCTION/ BACKGROUND

The Savannah River Site (SRS) Tritium Facilities have various process gas streams that contain impurities such as water, carbon monoxide, carbon dioxide, methane, and ammonia. Removal of tritiated impurities is needed to minimize emissions from tritium processing facilities and removal of carbon oxides is needed to prevent poisoning or consumption of process beds.

New SRS tritium facility projects will process impurities using a SAES® St909 bed before hydrogen isotope removal by diffusers. St909 is a Zr-Mn-Fe alloy getter material developed to dissociate, or "crack", tritiated water for tritium recovery[1], and retain relatively low amounts of hydrogen.[2] This getter has been demonstrated to remove carbon monoxide and carbon dioxide from inert streams[3] as well as oxygen, and to crack ammonia and methane.[4,5] St909 is supplied as a single phase ZrMnFe alloy with an aluminum binder for pellet formation. Its composition is 40.5 wt% Zr, 24.5 wt% Mn, 25 wt% Fe, and 10 wt% Al.

Methane was found to be the most difficult impurity to process[6] and can impact diffuser operation.[7] The most systematic study of methane cracking by St909 used 0.1% and 1.0% methane in a helium carrier gas over a range of operating conditions.[5] That work was recently extended to higher methane concentrations[8] and examined bench scale methane cracking efficiency (ε_M) in carrier gases of helium, hydrogen, and nitrogen.[8] In this work, bench scale cracking tests were performed to examine the effect of carbon dioxide on ε_M and to determine carbon dioxide cracking efficiencies (ε_{CO2}) in different carrier gases. The effect of ammonia on ε_M and ε_{CO2}, and the effect of methane and carbon dioxide on ammonia cracking efficiency (ε_A) were also explored.

Definitions

The efficiency of a reactor can be defined as the difference between the concentration of a species entering and exiting the reactor divided by the concentration entering the reactor. The methane cracking efficiency, ε_M, is calculated using

$$\varepsilon_M = \frac{C_{CH4,in} - C_{CH4,out}}{C_{CH4,in}} = 1 - \frac{C_{CH4,out}}{C_{CH4,in}} = 1 - \frac{I_{CH4,b,out}}{I_{CH4,b,in}} \quad (1)$$

where C is gas stream concentration (proportional to partial pressure), the subscripts in and out represent bed gas sampling location, and $I_{a,b}$ the residual gas analyzer (RGA) ion current of species a at mass b.

There is a difference between efficiency and fractional conversion, which is usually used when calculating reaction equilibria. The methane fractional conversion, x_M, is defined as

$$x_M = \frac{N_{CH4,in} - N_{CH4,out}}{N_{CH4,in}} = 1 - \frac{N_{CH4,out}}{N_{CH4,in}} = 1 - \frac{F_{out}\, C_{CH4,out}}{F_{in}\, C_{CH4,in}} = 1 - \frac{F_{out}\, I_{CH4,b,out}}{F_{in}\, I_{CH4,b,in}} \quad (2)$$

where N_{CH4} is the moles of methane and F is the total volumetric gas flow. The difference between x_M and ε_M is that x_M is based on mass (moles) and ε_M is based on concentration. For reactions with a net change in moles of gas, these two quantities will be different. Efficiencies

were calculated since the total volume of gas exiting the bed could not be accurately measured using existing instruments.

The carbon dioxide cracking efficiency, ε_{CO2}, is calculated using

$$\varepsilon_{CO2} = \frac{C_{CO2,in} - C_{CO2,out}}{C_{CO2,in}} = 1 - \frac{C_{CO2,out}}{C_{CO2,in}} = 1 - \frac{I_{CO2,b,out}}{I_{CO2,b,in}} \tag{3}$$

RGA analysis of carbon dioxide produces a mass 28 carbon monoxide fragmentation species. Getter tests with carbon dioxide produced mass 28 signals greater than the carbon dioxide fragmentation signal and was attributed to the formation of carbon monoxide during the test. A combined carbon dioxide plus carbon monoxide cracking efficiency, $\varepsilon_{COX,}$ equals $\varepsilon_{(CO2+CO)}$, is calculated using

$$\varepsilon_{COX} = \frac{(C_{CO2} + C_{CO})_{in} - (C_{CO2} + C_{CO})_{out}}{(C_{CO2} + C_{CO})_{in}} = \frac{\varepsilon_{CO2} + C_{CO,in} / C_{CO2,in} - C_{CO,out} / C_{CO2,in}}{1 + C_{CO,in} / C_{CO2,in}} \approx \varepsilon_{CO2} - \frac{C_{CO,out}}{C_{CO2,in}} \tag{4}$$

The approximation was derived by setting $C_{CO,in}$ to zero since carbon monoxide was not part of the test feed mixtures other than as a trace impurity. The method to calculate ε_{COX} using RGA ion currents is discussed in Appendix A.

Concentrations calculated from feed conditions and efficiencies can be derived and used to calculate outlet partial pressures:

$$C_{CH4,out} = C_{CH4,in}(1 - \varepsilon_M) \tag{5}$$

$$C_{CO2,out} = C_{CO2,in}(1 - \varepsilon_{CO2}) \tag{6}$$

$$C_{CO,out} = C_{CO2,in}(\varepsilon_{COX} - \varepsilon_{CO2}) \tag{7}$$

The carbon gettering or loading of the material, $St909_C$, can be expressed as:

$$St909_C = \int_0^t F_{CH4,in}\, \varepsilon_M\, dt + \int_0^t F_{CO2,in}\, \varepsilon_{COX}\, dt \tag{8}$$

where $F_{CH4,in}$ and $F_{CO2,in}$ represent the flow rate of methane and carbon dioxide into the getter bed. The oxygen (O) loading of the material, $St909_O$, is calculated using

$$St909_O = \int_0^t 2 * F_{CO2,in} \left(\varepsilon_{CO2} - \frac{1}{2} \frac{FF_{CO2,28} XF_{CO2}}{FF_{CO,28}\, XF_{CO}} \left[\frac{I_{ALL,28}}{I_{CO2,28,feed}} - \frac{I_{CO2,44}}{I_{CO2,44,feed}} \right] \right) dt \tag{A9}$$

with the terms in the equation defined in Appendix A. The total impurity loading, $St909_T$, is the sum of the carbon and oxygen loadings:

$$St909_T = St909_C + St909_O \tag{9}$$

EXPERIMENTAL

Baseline test conditions were 5 (volume) % methane with helium carrier gas, a feed rate of 10 sccm, 760 torr back-pressure, and 700°C. Helium, hydrogen, nitrogen, and a 1.99% ammonia/balance helium gas mix were carrier gases used with a mix of 99% methane with an argon tracer gas, and/or a mix of 98.5% carbon dioxide with a krypton tracer gas.

The test bed was made from 9.53 mm (3/8 inch) O.D., 0.889 mm (0.035 inch) wall, bright-annealed 316L stainless steel (SS) tubing. The St909 was nominal 6 mm O.D. by 4 mm tall cylindrical pellets, weighing approximately 0.6 grams each, with ten fresh pellets used for each test. A SS filter cup compressed in the bottom supported the pellets. At room temperature, the pellets occupied 61 % of the cross-sectional area of the bed, giving a void volume of 0.728 cc, and a bed residence time of 1.2 seconds at baseline conditions.

A simplified test system schematic, which used 3.18 mm (1/8 inch) O.D. by 2.16 mm (0.085 inch) I.D. 316 SS tubing and gas chromatographic (G.C.) valves to reduce dead volume, is shown in Figure 1. The G.C. valves functioned like two, three-way ball valves in their ability to valve-in or bypass a piece of equipment.

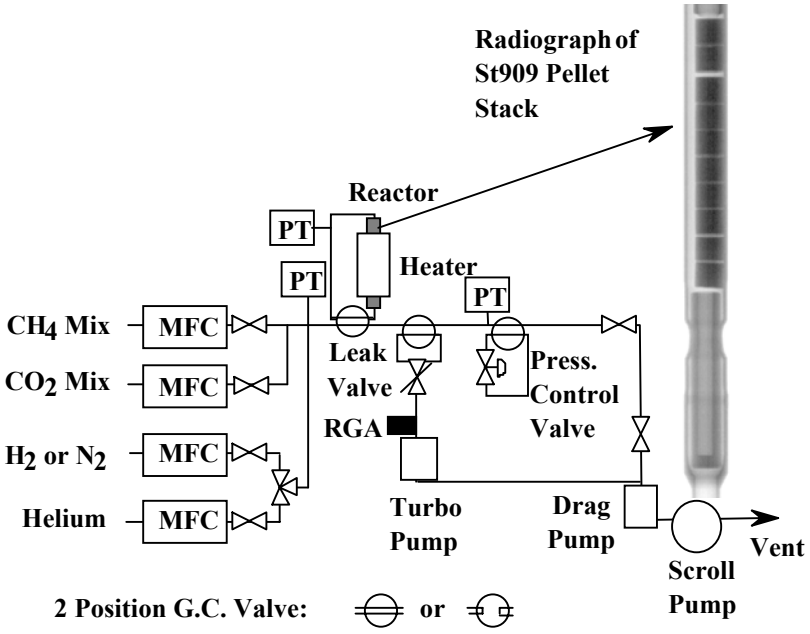

Figure 1. Simplified Test System Schematic

Calibrated mass flow controllers (MFCs), with standard conditions of 760 torr and 0°C, supplied the feed gas into the top of the bed. Methane, carbon dioxide, and ammonia compositions are nominal values that are 99%, 98.5%, and 95.5% of the reported values due to the use of gas mixes. Pressure transducers (PTs) measured system pressures and provided feedback for the pressure control valve. A Leybold Inficon model TSPTT100 residual gas analyzer (RGA), atomic mass unit range up to mass 100, was used for testing. Lag-time tests with an empty test

bed filled with helium at ambient temperature and displaced with argon showed approximately seven minutes were needed for the RGA helium signal to decay to its baseline value.

Argon in the methane supply and krypton in the carbon dioxide supply allowed ε_M and ε_{CO2} to be calculated on a relative basis using RGA ion currents, eliminating the need for RGA calibrations to derive gas concentrations. RGA data were collected for the feed gas before and after the test with the effluent monitored continuously during testing. The 16/40, 15/40, or the 13/40 mass ratio of the bed inlet gas and effluent were used to calculate ε_M, the 44/84 mass ratio for ε_{CO2}, and the 17/4 or 17/40 mass ratio used to calculate ε_A. The ion current ratios of the feed gas before and after a test were averaged for calculating efficiencies and varied only a few percent.

The pellets were evacuated to less than 1.33 Pa ($1x10^{-2}$ torr) and activated at 600°C for two hours with a ten sccm helium flow. The majority of tests were performed with 5% gaseous carbon impurities. A three-by-three test matrix was constructed with carbon impurities of 5% methane, 2.5% methane plus 2.5% carbon dioxide (denoted as the "2.5%+2.5%" mixture), and 5% carbon dioxide with carrier gases of helium, hydrogen, or nitrogen. Tests were run at 760 torr, 10 sccm total flow, for 27 hours at 700 °C unless stated otherwise. Tests using only 2.5% methane or carbon dioxide were run 54 hours to expose the getter to the same amount of impurities. A series of tests were also run with the helium carrier gas replaced with a 2% ammonia in helium carrier gas to measure ε_A and determine the impact of ammonia on ε_M and ε_{CO2}. After a test, the pellets were evacuated, purged with helium for nine minutes, isolated, cooled to ambient temperature, and analyzed.

RESULTS

Cracking efficiencies were plotted versus cumulative volume (standard cm^3: scc) of gaseous carbon species (methane plus carbon dioxide) fed to the bed. This is similar to plotting the data versus time except for tests with 2.5% impurities which were run twice as long. Some results were also plotted versus carbon gettered by the bed ($St909_C$). End-of-test increases in cracking efficiencies were attributed to the increased pressure drop across the bed required to maintain constant feed flow rate and constant bed outlet pressure. Tests with carbon dioxide, which included ammonia or nitrogen in the feed gas, did not allow accurate calculation of ε_{COX} or getter loadings due to the inability to differentiate nitrogen from carbon monoxide at mass 28. Results with ammonia in the feed gas gave lower ε_{COX} and getter loadings since the nitrogen released from ammonia cracking was treated as carbon monoxide. Results are for 700°C unless indicated otherwise.

Helium Carrier

Figure 1a and Figure 1b show the effect of feed composition and temperature on ε_M versus carbon fed and carbon gettered, respectively. Without carbon dioxide in the feed, ε_M increased slightly as feed concentration decreased, but increased greatly with increased temperature. Figure 1b shows, with carbon dioxide added to the methane, ε_M was attenuated approximately 15% at the peak of the "min-max" (140 scc fed), but then decreased faster than the test without carbon dioxide. Adding 2% ammonia to the 2.5%+2.5% mixture had only a slight impact on ε_M: a slightly greater reduction than adding 2% ammonia and 2.5% methane to 2.5% methane. At 800°C, adding carbon dioxide reduced ε_M, especially after gettering approximately 350 scc of carbon.

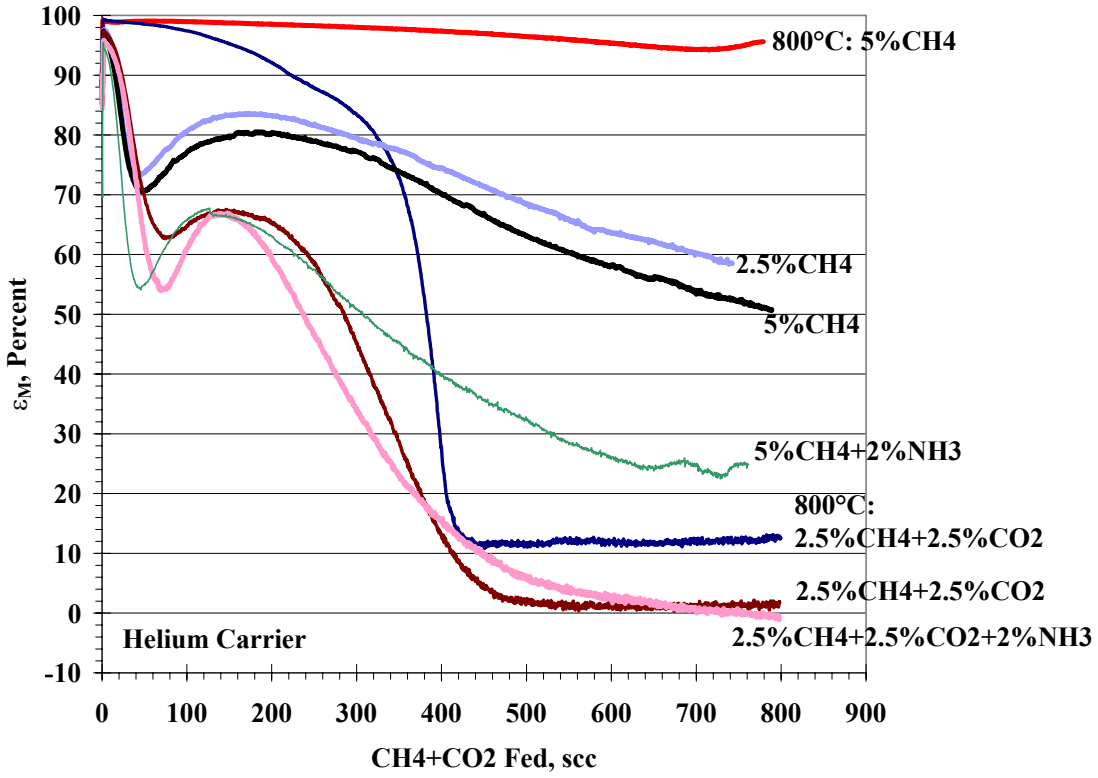

Figure 1a. Effect of Composition and Temperature on ε_M in Helium: Carbon Fed.

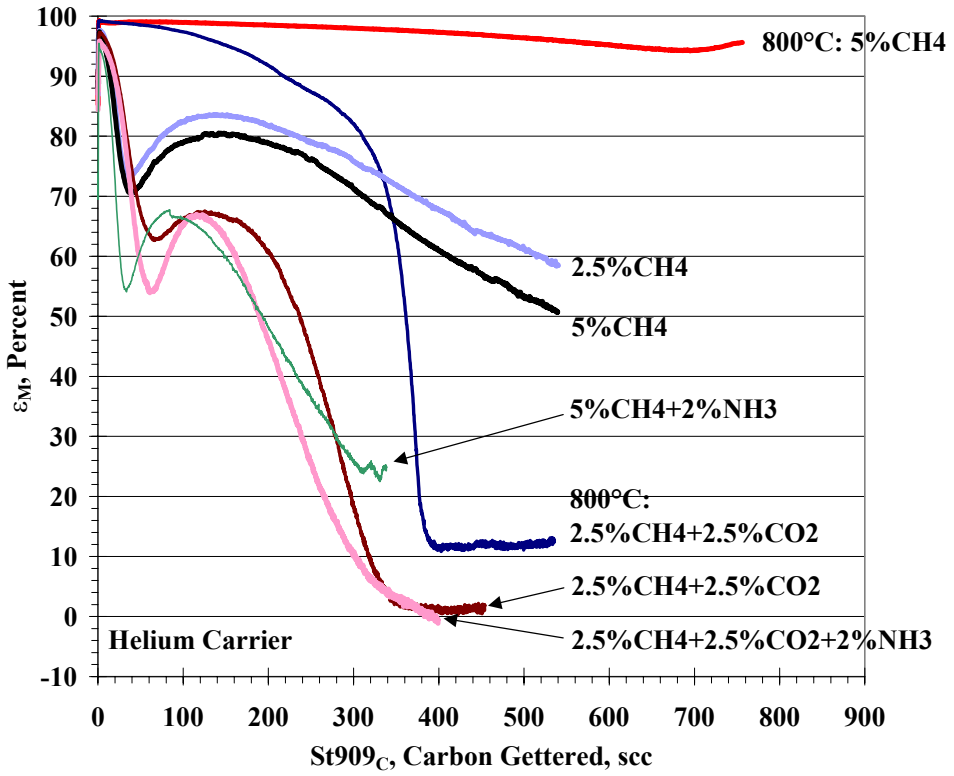

Figure 1b. Effect of Composition and Temperature on ε_M in Helium: Carbon Gettered.

For 5% methane, adding 2% ammonia to the feed decreased $\varepsilon_{M,}$ but the ε_M plots in Figures 1a and 1b show similar slopes. For the 2.5%+2.5% mixture in helium at 800°C, ε_M was initially greater than at 700°C, but then was reduced to a nearly constant value which was approximately 10% higher than ε_M at 700°C.

Figures 2a and 2b show ε_{CO2} and Figures 3a and 3b show ε_{COX} for tests with a helium carrier. Figure 2a shows ε_{CO2} remained above 86% for all tests in helium, but Figures 3a and 3b indicate significant amounts of carbon monoxide exited the getter bed.

Compared to 2.5% carbon dioxide feed, Figure 2b shows adding 2.5% carbon dioxide to the feed had little impact on ε_{CO2}, but adding an additional 2.5% methane delayed the decrease in ε_{CO2}. Adding 2% ammonia to the 2.5%+2.5% mixture appeared to delay the decrease in ε_{CO2} for the last part of the test in Figure 2a, but when plotted as a function of carbon gettered in Figure 2b, ε_{CO2} was almost the same for both tests. For 5% carbon dioxide feed, adding 2% ammonia increased ε_{CO2} for the last part of the test. Increasing the temperature increased ε_{CO2}.

Figures 3a and 3b show the effects of feed composition and temperature on ε_{COX} (note, test results with ammonia are approximate due to nitrogen mass 28 interference with carbon monoxide). The gradual decreasing slope in ε_{COX} plots for tests with ammonia were attributed to the increase in the mass 28 signal from ammonia cracking while the greater decreasing slopes later in the plots were attributed to the increases in the mass 28 signals from carbon monoxide formation.

Figure 3b shows ε_{COX} remained near 100% until a nominal 260 to 400 scc of carbon have been gettered by the bed after which there were rapid decreases in ε_{COX}. There is little difference between ε_{COX} when 2.5% carbon dioxide feed was increased to 5% at 700°C, or even at 800°C. Adding 2.5% methane to the 2.5% carbon dioxide feed delayed slightly the initial decrease in ε_{COX}; increasing the temperature to 800°C of this 2.5%+2.5% mixture further delayed the initial decrease in ε_{COX}, after which ε_{COX} decreased rapidly as with the other tests. Qualitatively, the addition of 2% ammonia to the feed mixture did not appear to significantly affect ε_{COX}.

In Figures 1a and 1b, adding carbon dioxide or ammonia to methane decreased ε_M, but adding both carbon dioxide and ammonia did not decrease ε_M further than adding just one of these gases to the methane. Conversely, adding methane or ammonia to carbon dioxide increased ε_{CO2}, and adding both methane and ammonia to carbon dioxide further increased ε_{CO2}. The addition of methane to carbon dioxide increased ε_{COX}, but the impact on carbon monoxide release when adding ammonia was less definitive due to the difficulty differentiating between nitrogen and carbon monoxide.

Ammonia Cracking

Figure 4 shows the effect of methane and carbon dioxide on ε_A. For comparison, Figure 4 shows ε_A when using only the 1.99% ammonia/helium carrier gas (no methane or carbon dioxide) when plotted versus total carbon (methane) fed when using this carrier gas with 5% methane.

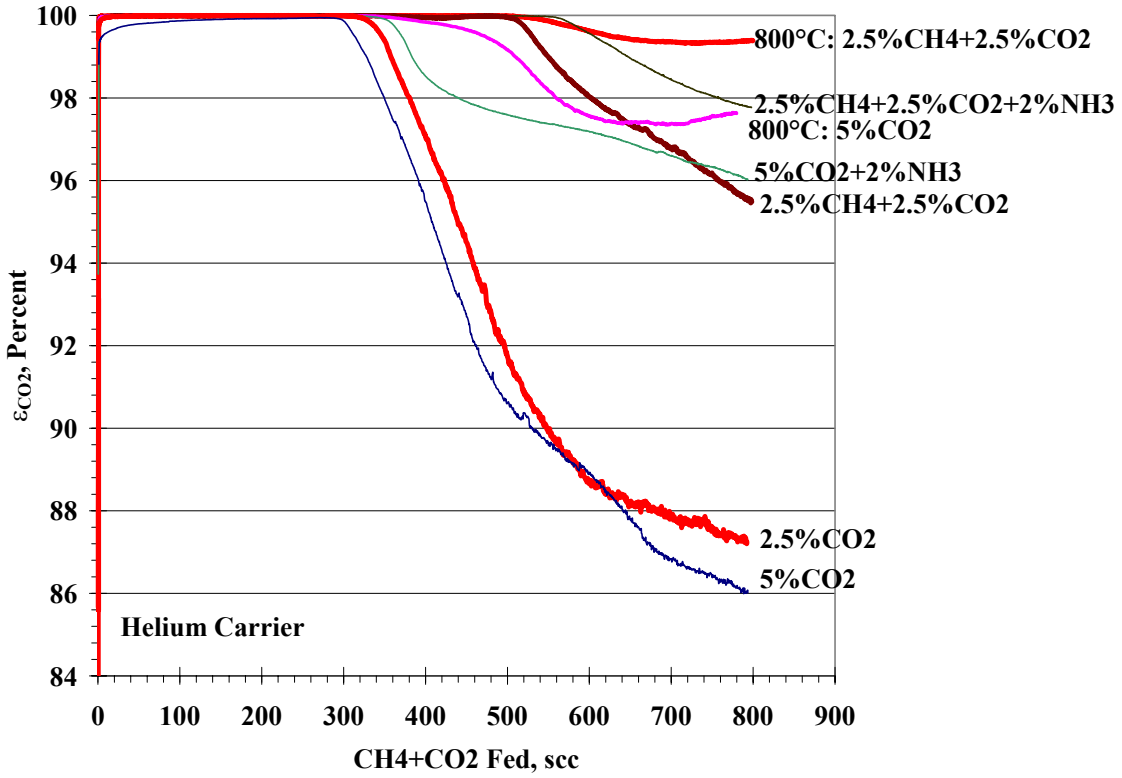

Figure 2a. Effect of Composition and Temperature on ε_{CO2} in Helium: Carbon Fed

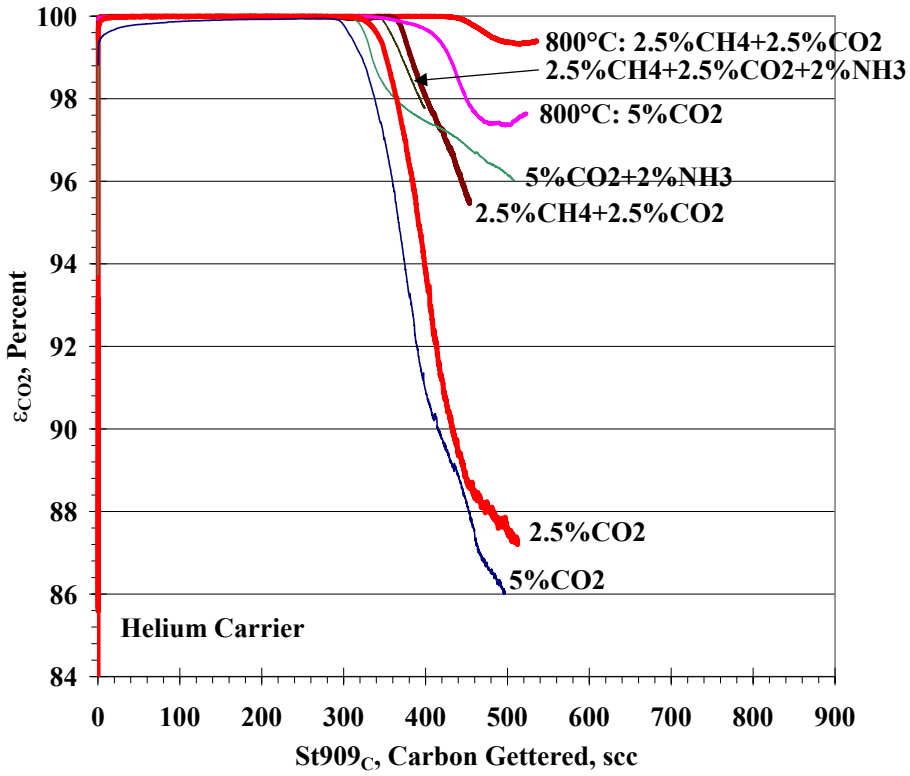

Figure 2b. Effect of Composition and Temperature on ε_{CO2} in Helium: Carbon Gettered.

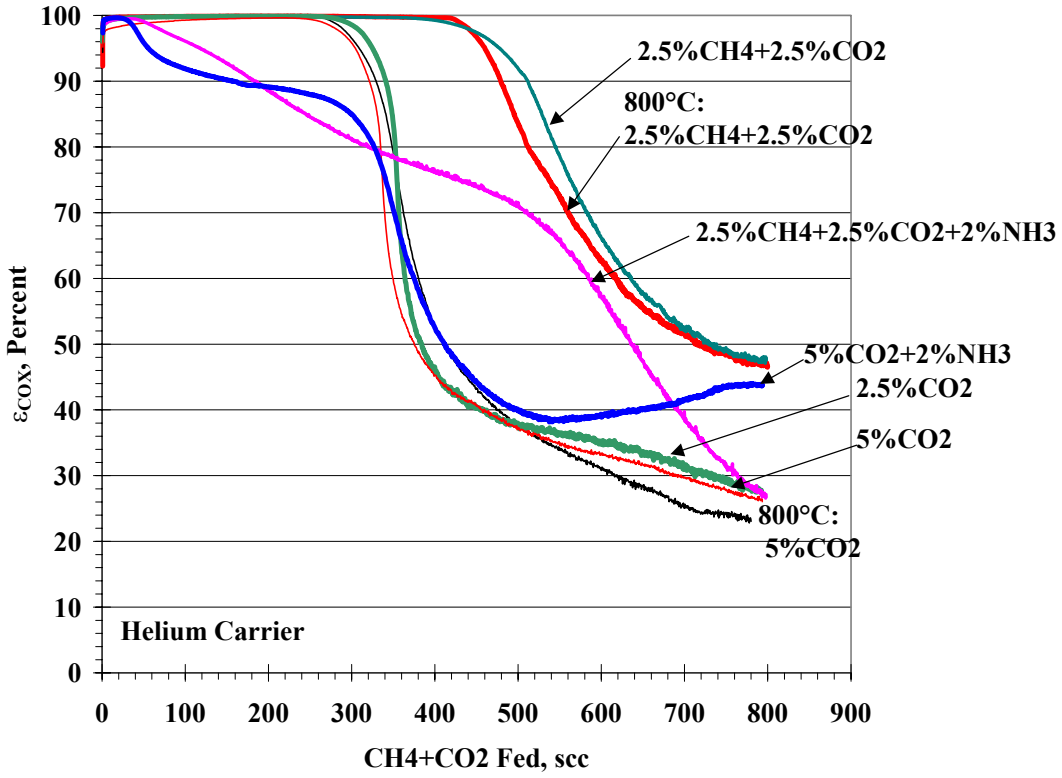

Figure 3a. Effect of Composition and Temperature on ε_{COX} in Helium: Carbon Fed.

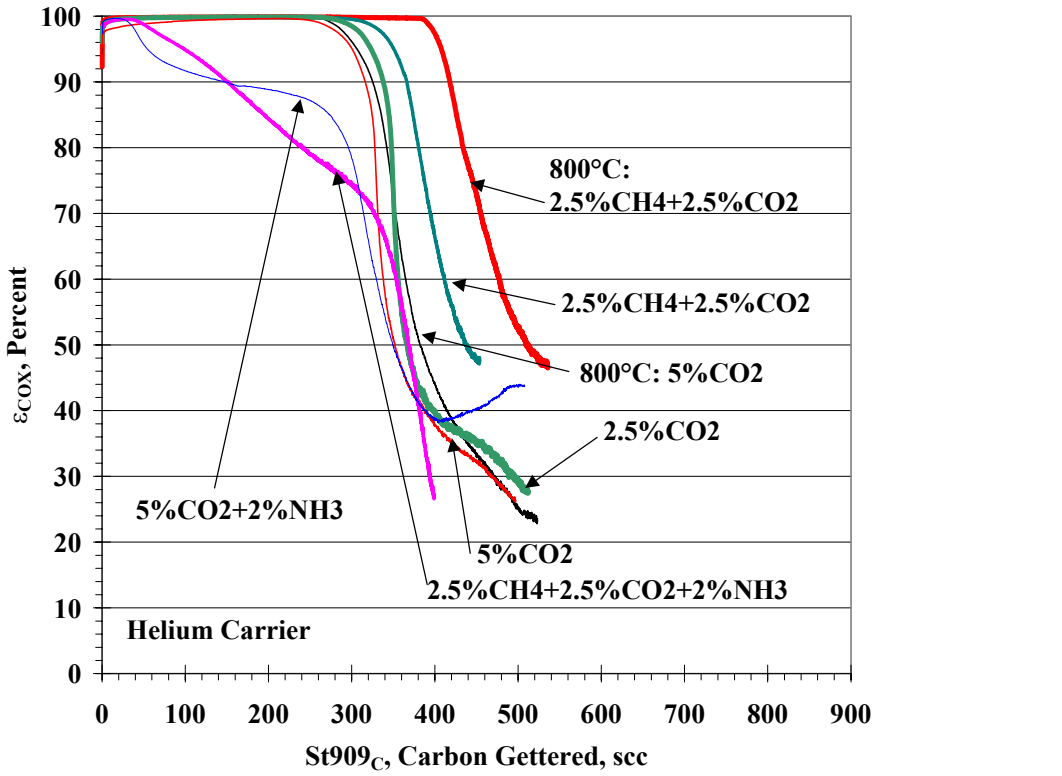

Figure 3b. Effect of Composition and Temperature on ε_{COX} in Helium: Carbon Gettered.

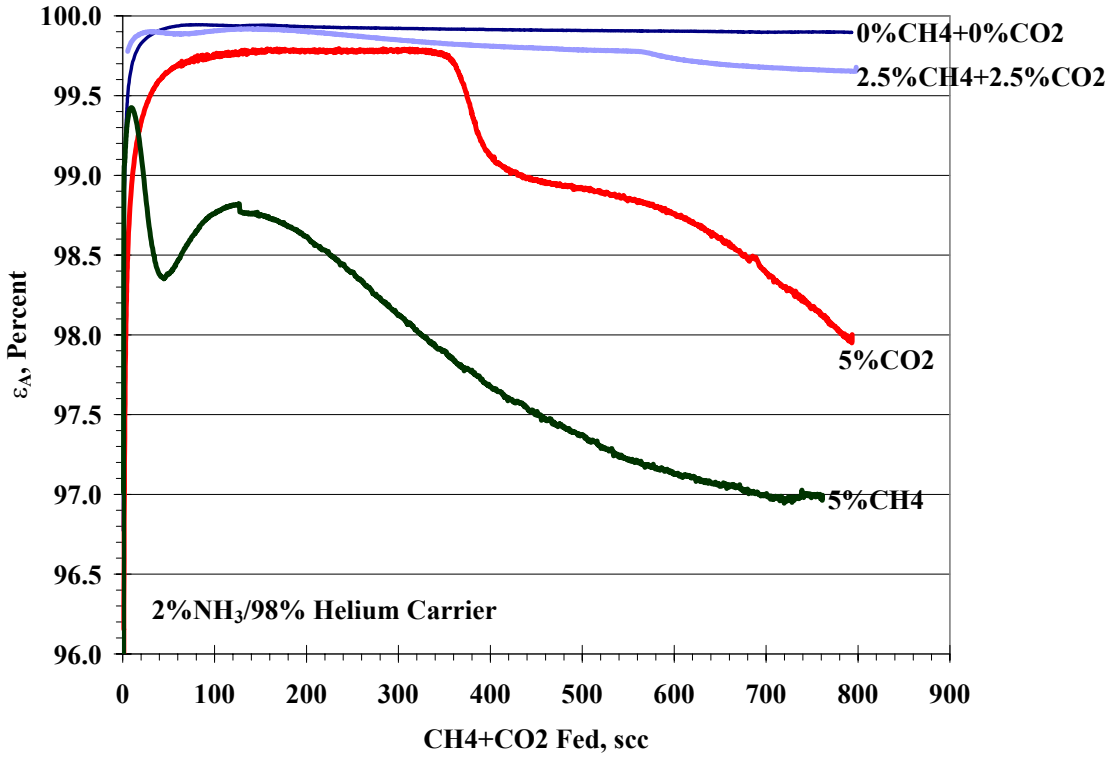

Figure 4. Effect of Methane and Carbon Dioxide on ε_A.

ε_A was nominally 97% or greater for all tests, was greatest without methane or carbon dioxide present, and was slightly reduced with the 2.5%+2.5% mixture. For 5% carbon dioxide feed, ε_A decreased from 99.8% to 99.2% at the same total carbon feed exposure as the Figure 2a ε_{CO2} decrease. The Figure 4 shape of the ε_A curve with 5% methane is similar to the Figure 1a shape of the ε_M curve with 5% methane and 2% ammonia: a min-max occurs in the efficiency plot.

Hydrogen Carrier

Figures 5a and 5b show the effect on ε_M when using a hydrogen carrier gas. The baseline test with the helium carrier gas is shown for comparison. ε_M was greatly reduced compared to using a helium carrier gas, but varied only slightly with methane composition. ε_M increased with increased temperature, but when carbon dioxide was added to the feed gas, ε_M became negative: more methane exited the bed than entered the bed.

At 700°C, the early, sharp decrease in the ε_M plot for the 2.5%+2.5% mixture was almost identical to the ε_M plot for 2.5% or 5% methane, but continued the rapid decrease in ε_M while the other plots changed to more gradual slopes. At 800°C, ε_M for the 2.5%+2.5% mixture started almost as high as ε_M for 5% methane at 800°C, but then decreased at a steeper rate.

Figure 6 shows ε_{CO2} while Figure 7 shows ε_{COX} as a function of carbon fed to the bed with a hydrogen carrier. The high values for ε_{CO2} and ε_{COX} ($\geq$ 99% and $\geq$ 84%, respectively) for all tests was attributed to a combination of gettering by the St909 and methane formation. Water formation was also detected in some tests.

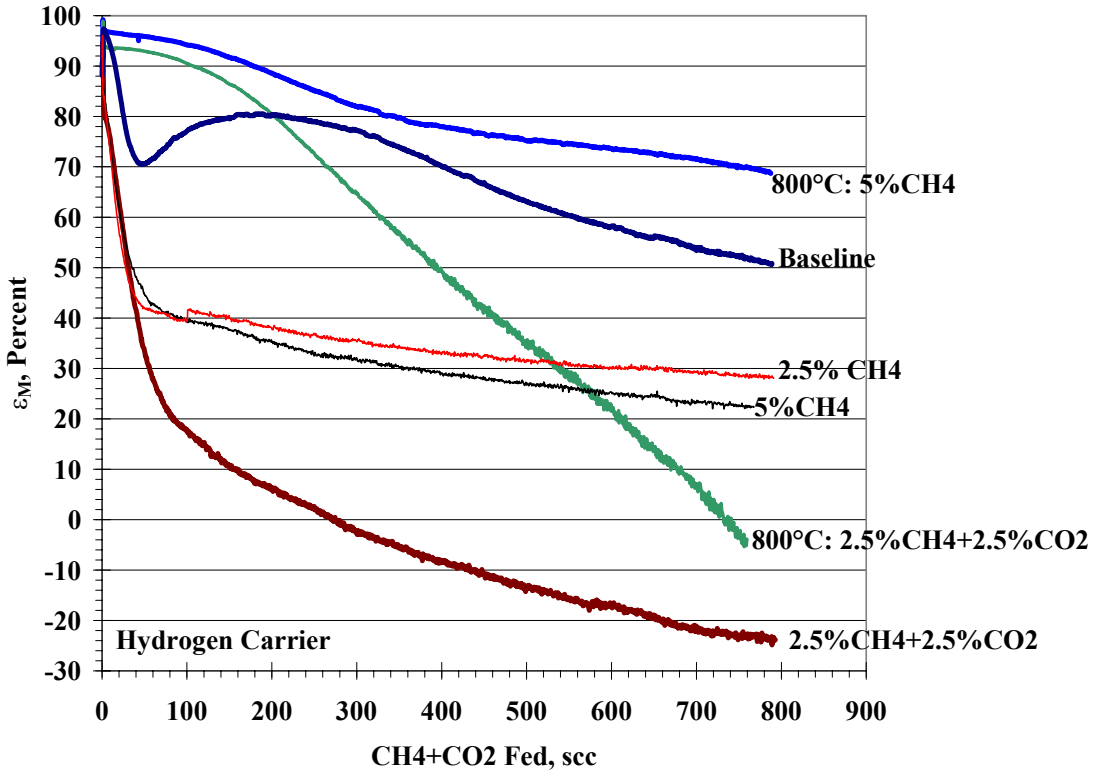

Figure 5a. Effect of Composition and Temperature on ε_M in Hydrogen: Carbon Fed.

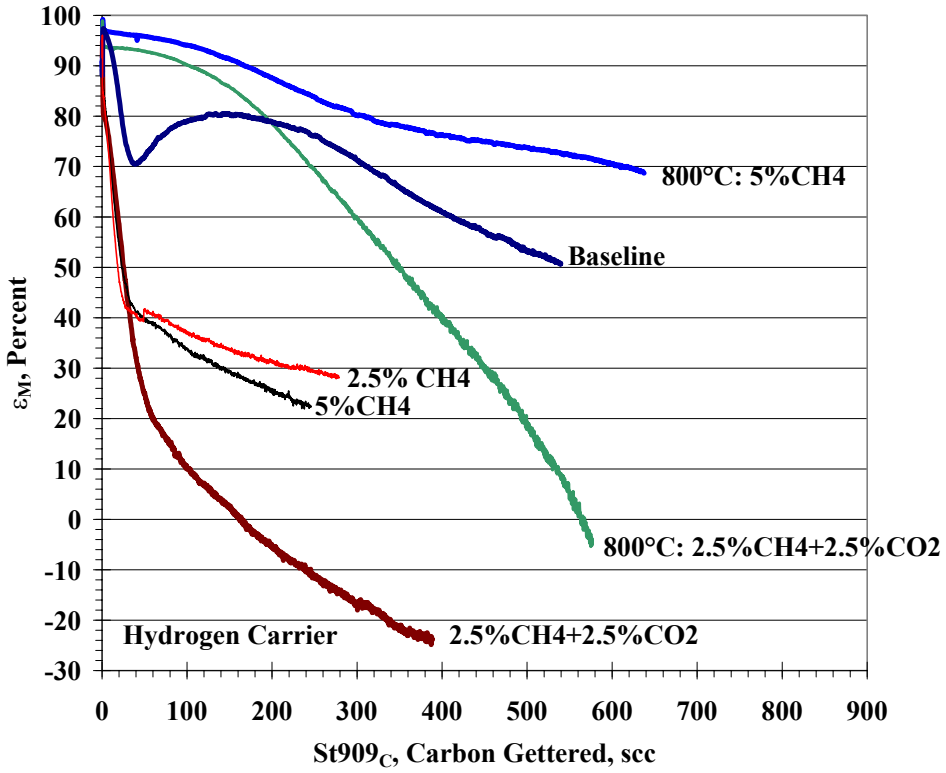

Figure 5b. Effect of Composition and Temperature on ε_M in Hydrogen: Carbon Gettered.

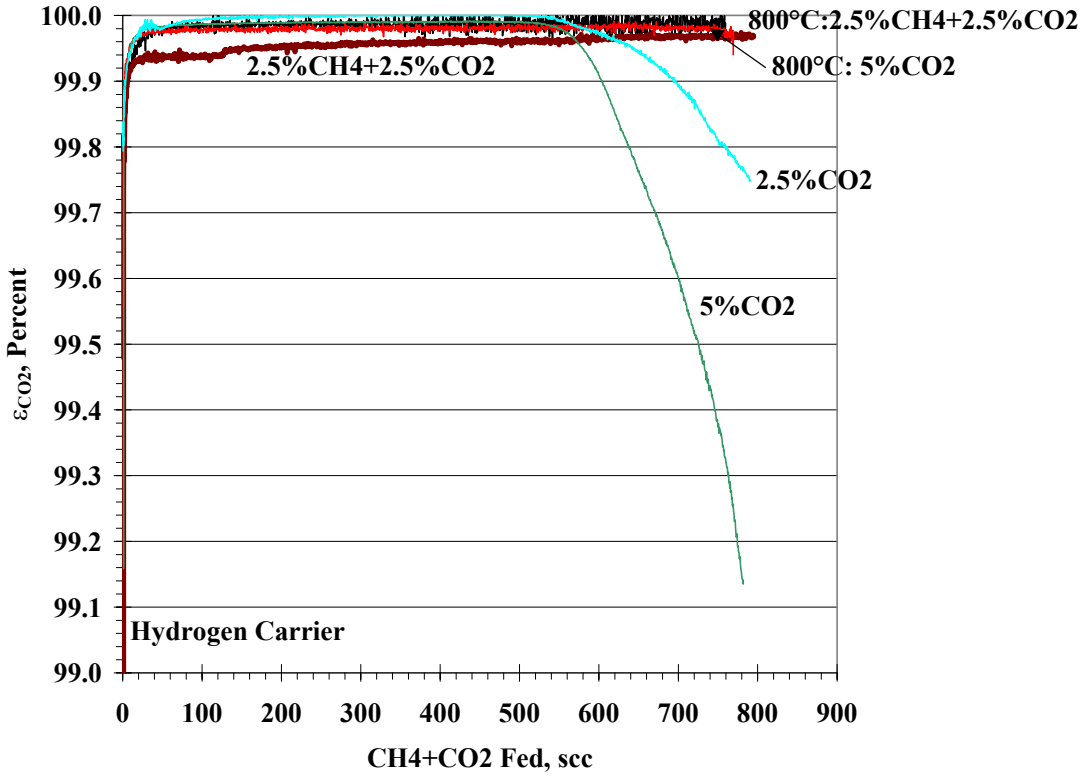

Figure 6. Effect of Composition and Temperature on ε_{CO2} in Hydrogen.

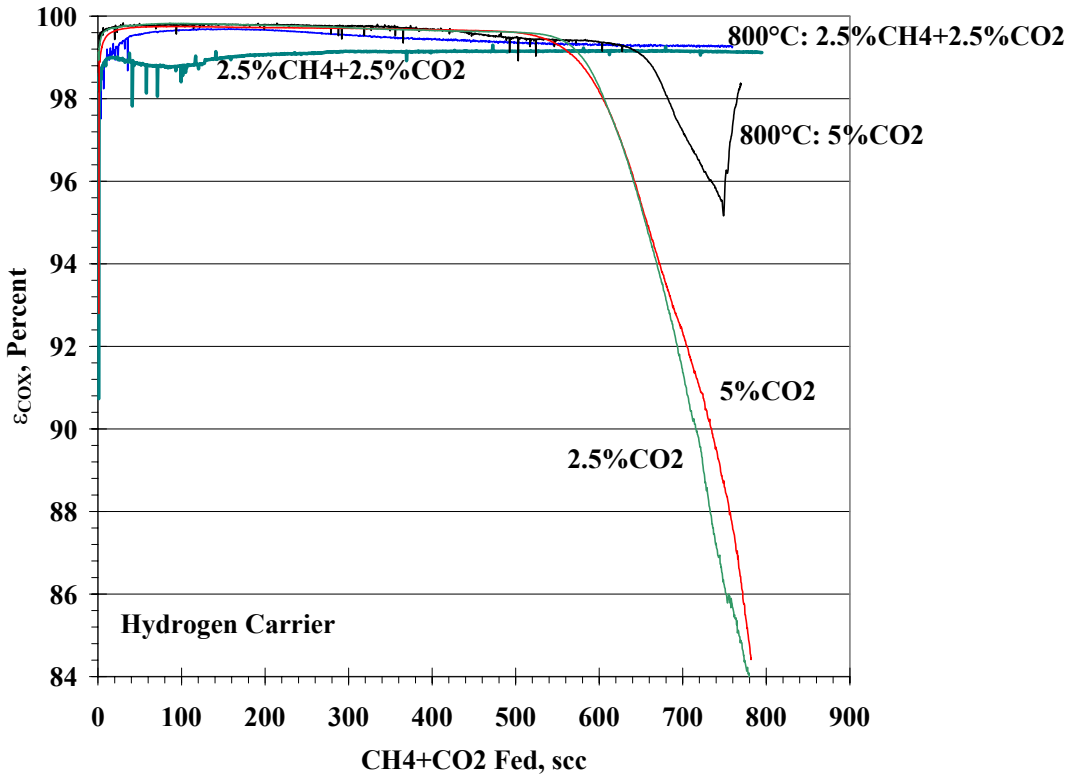

Figure 7. Effect of Composition and Temperature on ε_{COX} in Hydrogen.

Nitrogen Carrier

Figures 8 and 9 show the effect of feed composition and temperature on ε_M and ε_{CO2} in a nitrogen carrier gas: ε_{COX} could not be reliably calculated due to the large mass 28 signal from the nitrogen carrier and the significantly smaller increase in mass 28 signal from carbon monoxide formation. Figure 8 shows significantly lower ε_M values when using nitrogen compared to baseline test results with helium. Hydrogen from methane cracking did not react with the nitrogen carrier to form detectable concentrations of ammonia.

There was a modest difference in ε_M for methane concentrations, but the addition of carbon dioxide to the feed continued the initial decrease in ε_M seen with only methane at 700°C until ε_M approached near-zero values. It was not clear if the slight increase in ε_M after reaching the minimas shown in Figure 8 were due to increased pressure in the bed since the final pressure drop across the bed was approximately 4 torr greater than at the start of the test. Increasing the temperature to 800°C increased ε_M, but ε_M eventually approached values similar to those found at 700°C.

Figure 9 illustrates a nitrogen carrier gas caused the initial decrease in ε_{CO2} to occur at lower total carbon exposures and produce lower ε_{CO2} values than when using a helium carrier. As with a helium carrier, ε_{CO2} increased with increased temperature and showed little difference when the feed gas was 2.5% or 5% carbon dioxide. The addition of 2.5% methane to 2.5% carbon dioxide showed an increased ε_{CO2}, as was the case with the helium carrier.

Pellet Weight Change

Weight change profiles for individual pellets are shown in Figures 10, 11, and 12 for helium, hydrogen, and nitrogen carrier gases, respectively. The weight change profiles in the figures are relatively flat for tests when methane was the only test gas. Tests which included carbon dioxide had much steeper pellet mass profiles, with the inlet pellet (position 10) typically having the greatest increase. Data missing in Figure 10 for 2.5% carbon dioxide at 700°C were due to pellet breakage during removal from the test bed. Tests with a hydrogen carrier and carbon dioxide in the feed had the largest weight change and in many cases, the pellets could not be removed intact for analysis. Results for pellets that could not be analyzed individually are shown in Figure 11 as numerical averages for those pellets.

Bed mass changes were measured by pre- and post-test bed weighings and also estimated by time integrating gas flow/efficiency data. Mass gains were estimated for the decomposition of methane and carbon dioxide and mass losses estimated for carbon monoxide and methane, when formed, for helium and hydrogen carrier gases. The integrated mass of carbon dioxide cracked, using ε_{CO2}, was similar for helium or nitrogen carrier gases. As an approximation for tests with a nitrogen carrier, the amount of carbon monoxide released was assumed to be the same as for the corresponding test with a helium carrier gas. Figure 13 shows the difference in mass between bed weighings and gas composition integrations. Without the carbon monoxide mass adjustments, the carbon dioxide in nitrogen tests would have yielded integrated mass gains 5% to 6% greater than those obtained by bed weighings (negative –5% to –6% in Figure 13). The mass calculations were unable to account for the water formed during the tests.

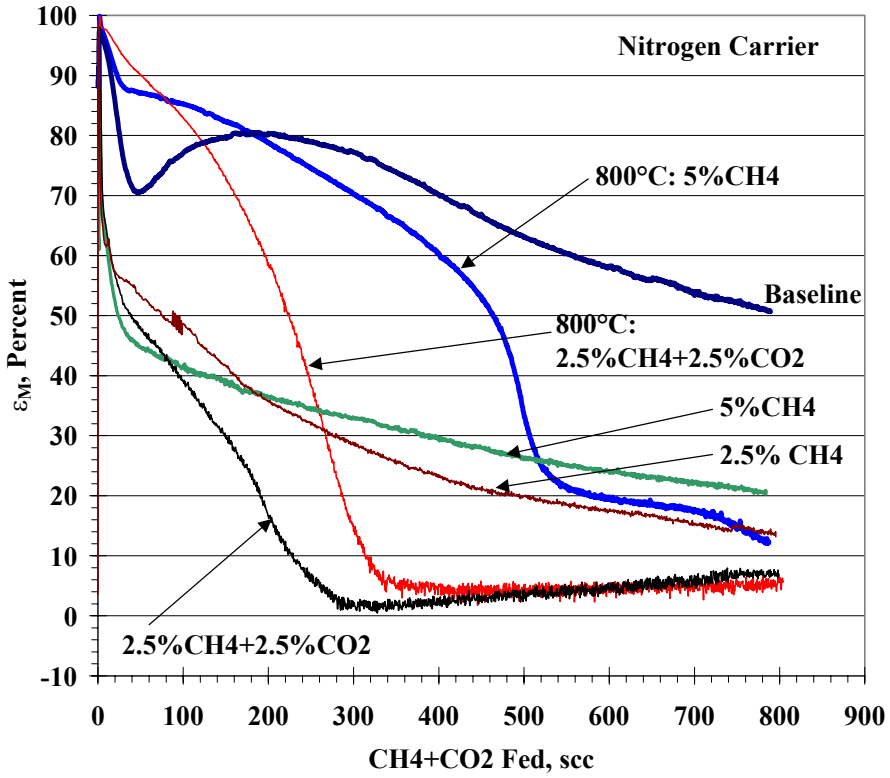

Figure 8. Effect of Composition and Temperature on ε_M in Nitrogen.

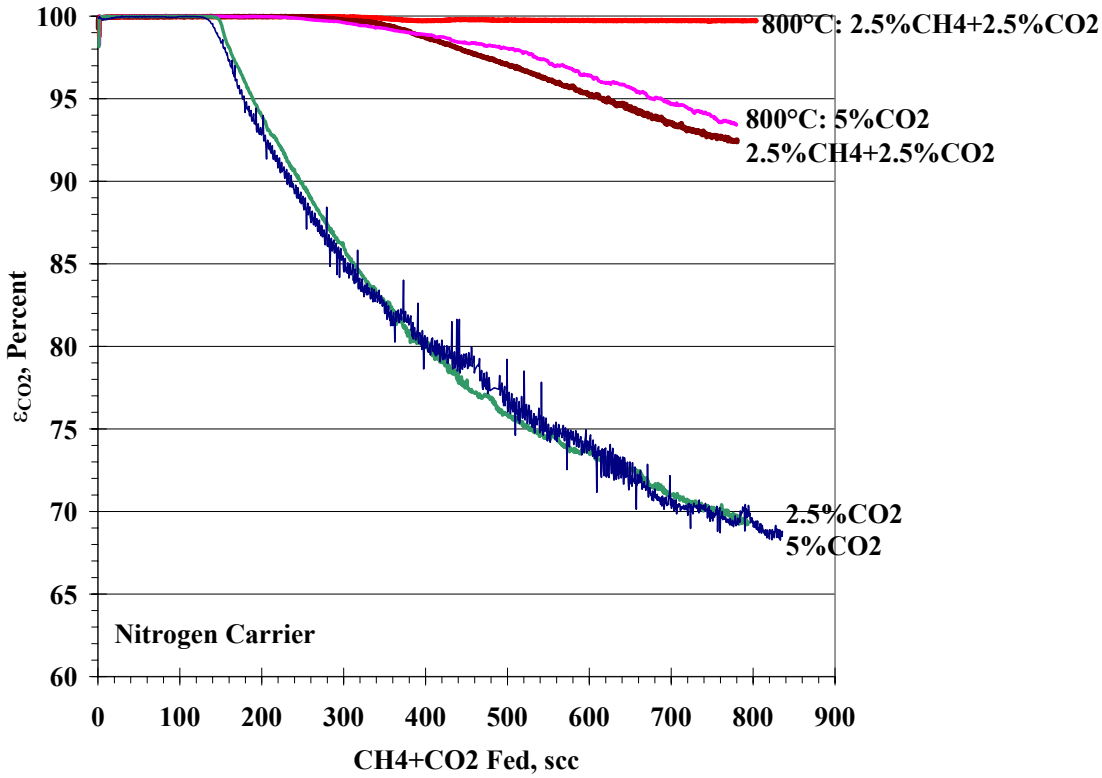

Figure 9. Effect of Composition and Temperature on ε_{CO2} in Nitrogen.

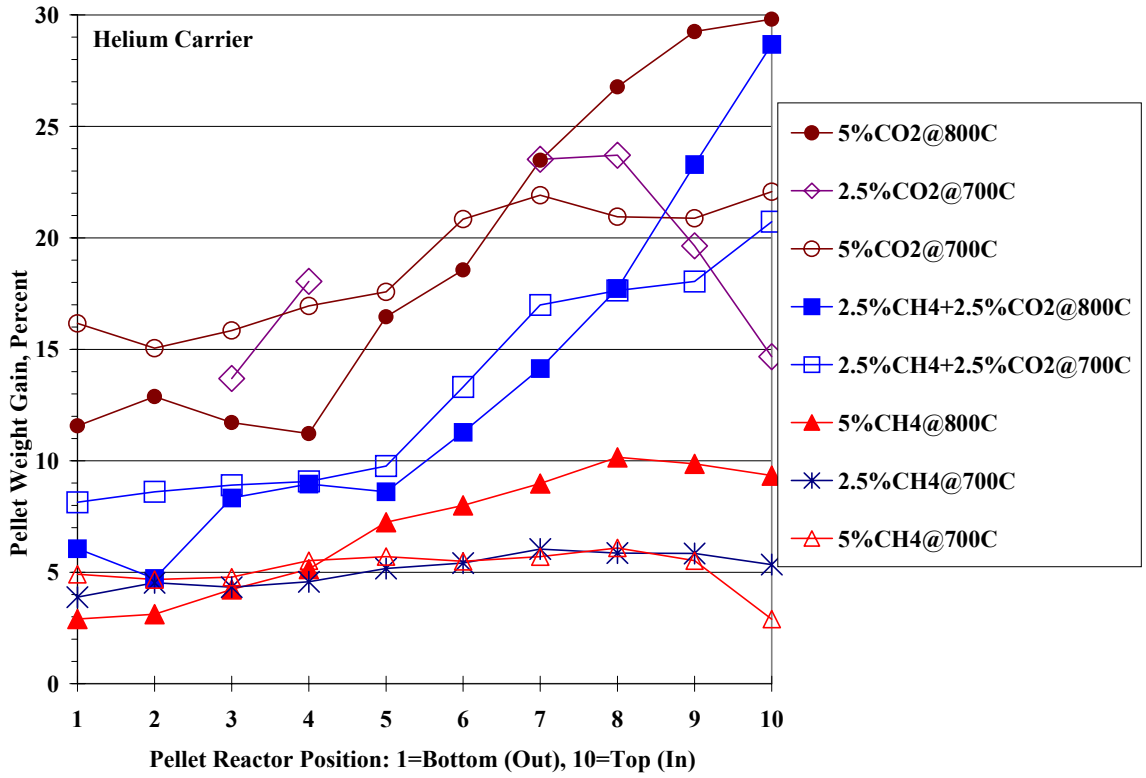

Figure 10. Pellet Weight Change with Helium Carrier

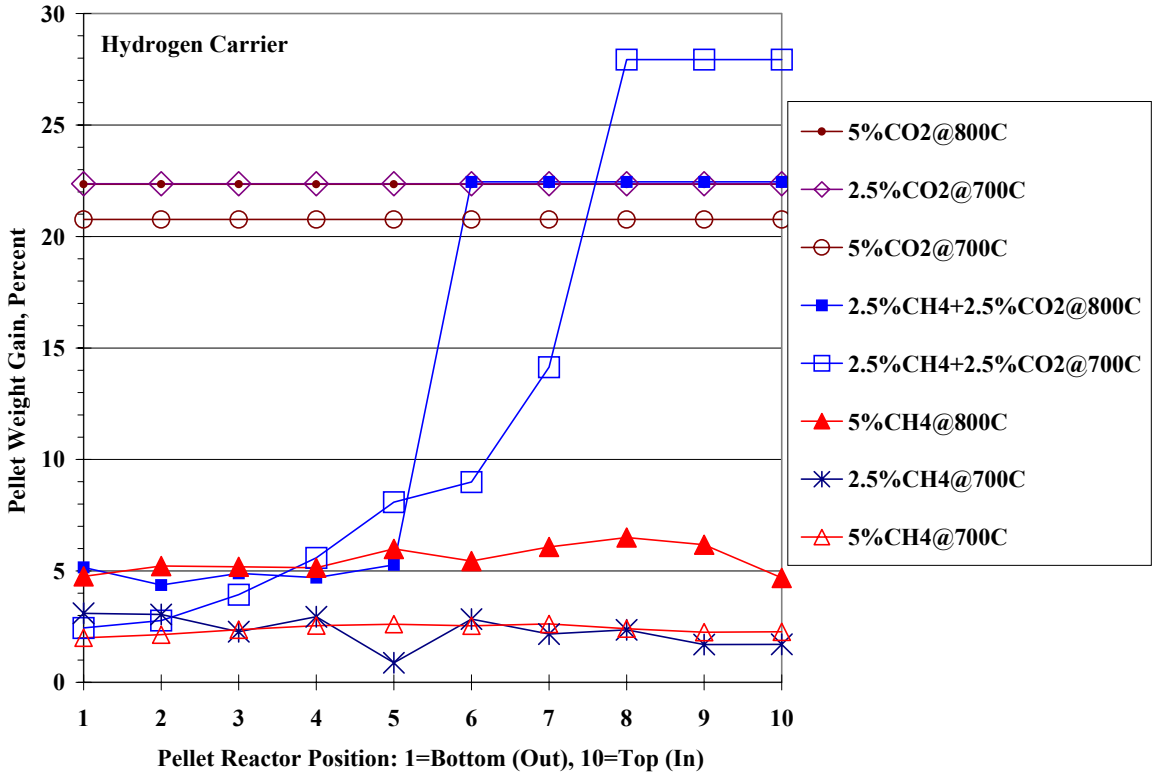

Figure 11. Pellet Weight Change with Hydrogen Carrier

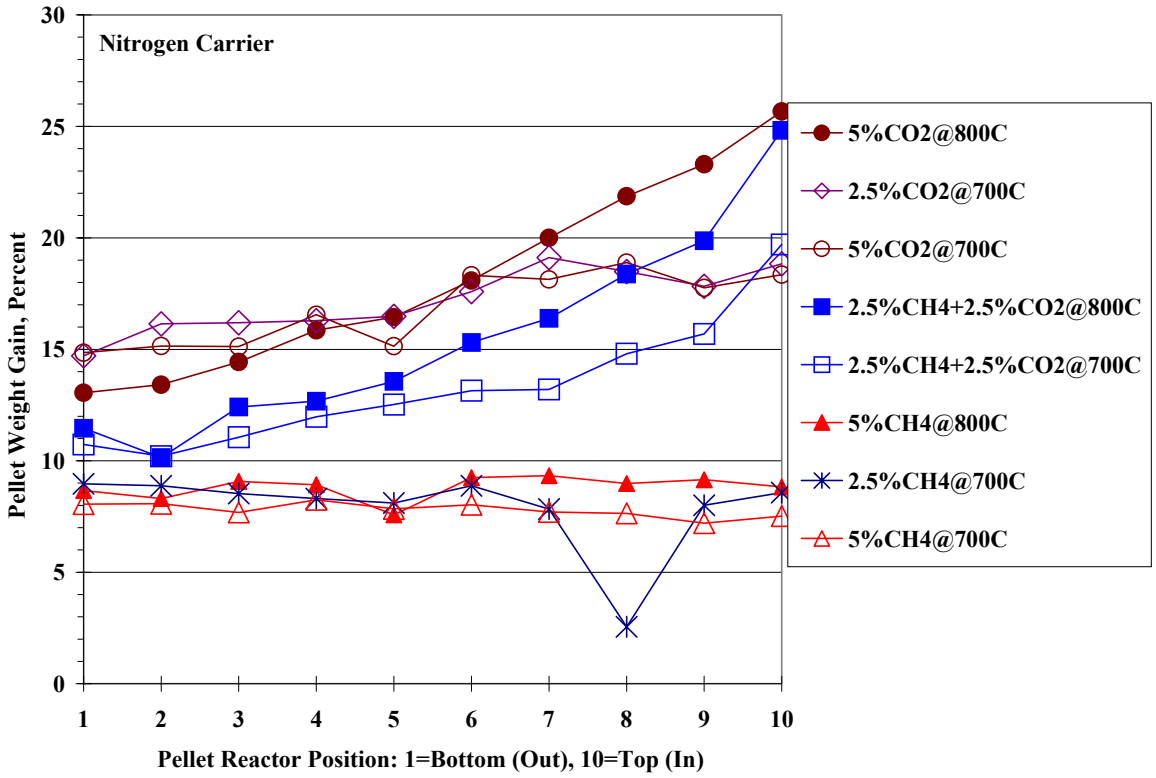

Figure 12. Pellet Weight Change with Nitrogen Carrier

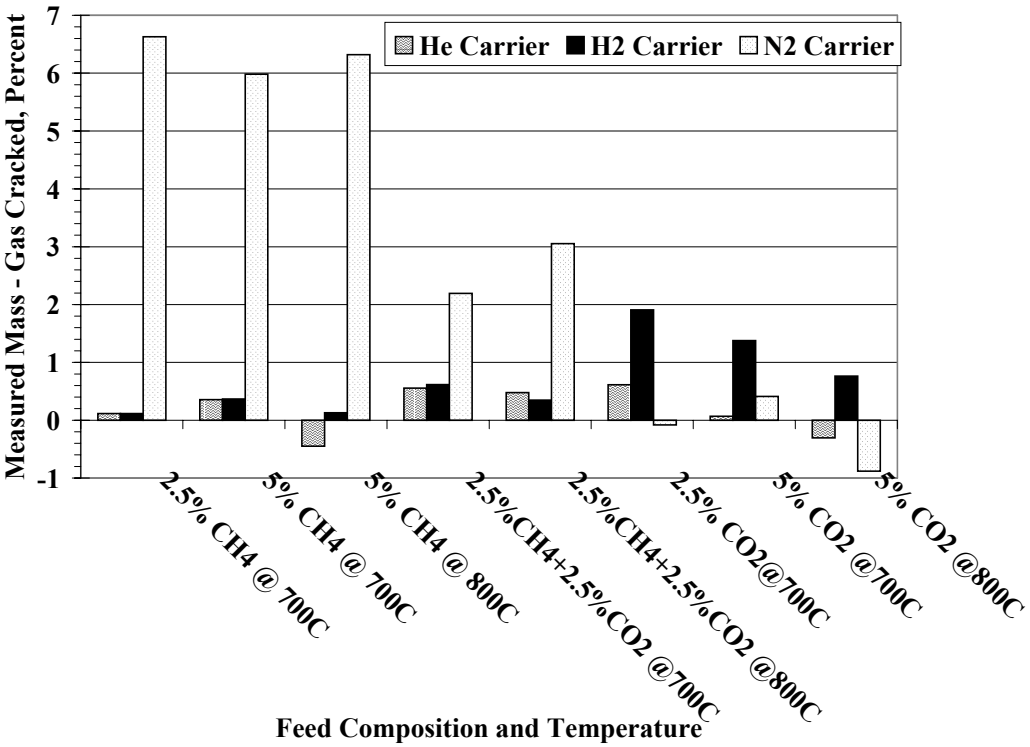

Figure 13. Weight Change with Different Compositions and Carrier Gases

Pellet and Bed Diameter Changes

Figure 14 shows pellet diameter change versus weight change: the legend identifies percent methane, percent carbon dioxide, the carrier gas, and the test temperature. Hydrogen carrier tests with carbon dioxide were not plotted due to the inability to remove the pellets for measurements; the 5% carbon dioxide test at 800°C swelled the bed O.D. at one location from 0.376 inches to 0.386 inches. Tests without carbon dioxide (symbols without lines), highlighted in Figure 14 by an oval, show no apparent correlation between weight and diameter change. Tests with carbon dioxide (symbols with lines) show a nominal 22% diameter increase per 30% weight increase.

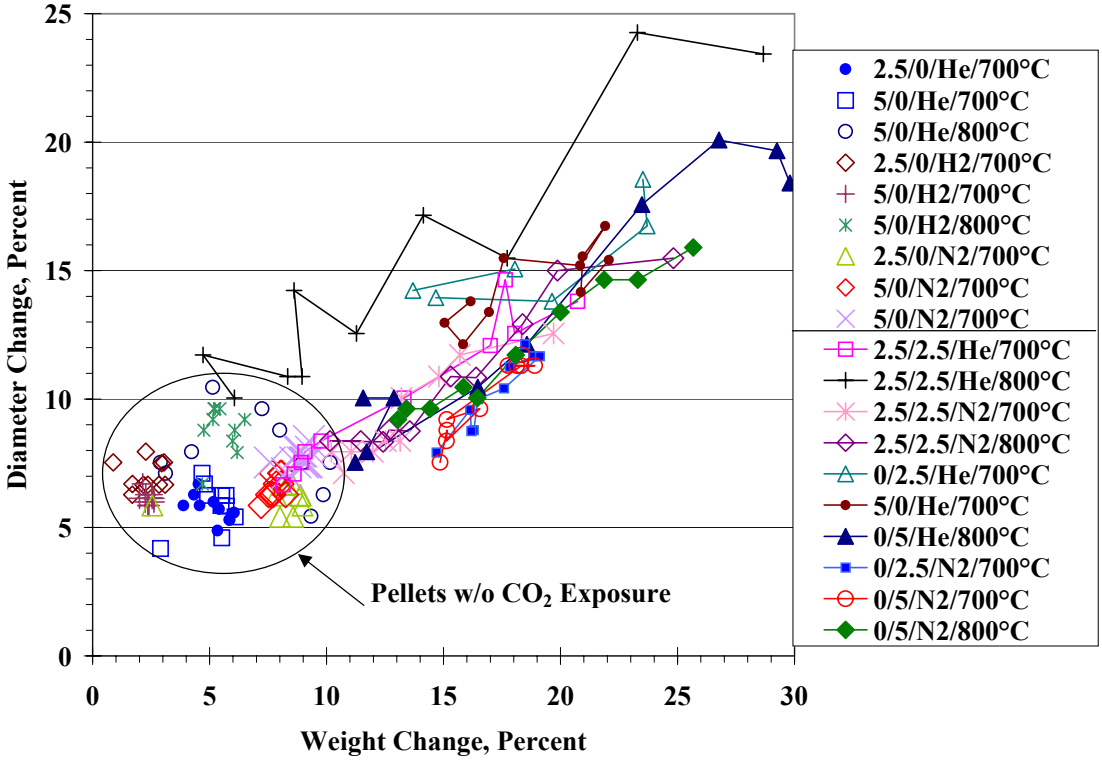

Figure 14. Pellet Diameter versus Weight Change

DISCUSSION

Methane Cracking

The gas phase methane decomposition, or "cracking", reaction can be written as

$$CH_4 \rightarrow C + 2H_2 \tag{10}$$

or can be written in terms of a getter as

$$CH_4 + 2M \rightarrow MC + M_{2xH} + (2-x)H_2 \quad x = 0,1,2 \tag{11}$$

where M generically stands for the metal getter, MC stands for some unspecified combination of M and carbon (carbon on the metal surface, dissolved in the metal, or as a metal carbide), and M_{2xH} stands for hydrogen solubility in M. Low hydrogen solubility was shown to be approximately 10 scc per 100 grams St909 between 700°C to 800°C[5] so methane decomposition will be written as

$$CH_4 + M(surface) \rightarrow MC(surface) + 2H_2 \quad (12)$$

$$MC(surface) + M(bulk) \rightarrow M(surface) + MC(bulk) \quad (13)$$

where metal-carbon species can exist on the surface or in the bulk of the metal. The reverse methane decomposition reaction, the methane reformation reaction, is written as

$$MC(surface) + 2H_2 \rightarrow CH_4 + M(surface) \quad (14)$$

$$M(surface) + MC(bulk) \rightarrow MC(surface) + M(bulk) \quad (15)$$

where carbon can be supplied to the surface for methane formation by the reverse of Equation 13.

Lower ε_M in a hydrogen carrier than a helium carrier can be explained in terms of a decreased equilibrium driving force for Equation 12.[8] At 700°C and 760 torr, 5% methane is in equilibrium with carbon, 61.9% hydrogen, and 33.1% helium while 2.5% methane is in equilibrium with carbon, 43.8% hydrogen, and 53.7% helium. Equation 12 is favored in a helium carrier while Equation 14 is favored in a hydrogen carrier unless carbon is removed by Equation 13 to allow Equation 12 to proceed.

Carbon removal from the getter surface, Equation 13, is not required for Equation 12 to proceed in helium so greater amounts of carbon can be created on the surface than in hydrogen. Larger amounts of carbon on the surface in helium than in hydrogen create larger gradients for Equation 13 producing larger ε_M values. Increased ε_M at increased temperature was attributed to increased rates of Equations 12 and 13.

Methane reformation via Equation 14 was demonstrated by cracking 5% methane in helium followed by flowing 9.5 sccm hydrogen through the bed. Figure 15 shows the 16/2 mass ratio during the hydrogen flow through the bed with the magnitude of the 16/2 ratio an indicator of the methane formation rate. Faster and greater methane formation at 700°C than at 800°C was supported by pellet weight gain data: the differences in post-test pellet masses between tests without and with the reforming hydrogen flow were greater at 700°C than at 800°C. A lower methane reformation rate at 800°C was attributed to lower surface carbon concentrations at 800°C due to Equation 13 being faster at 800°C than at 700°C during the cracking test and also during the hydrogen flow.

Figure 16 shows outlet methane, carbon monoxide, and carbon dioxide partial pressures, calculated using Equations 5, 6, and 7, for tests with helium versus total impurity loading ($St909_T$). A feed reactant partial pressure at 2.5% was 19 torr and is shown in the figure. Partial pressures for tests with only 5% methane or carbon dioxide were divided by two for comparison to tests containing 2.5% of the carbon containing gas.

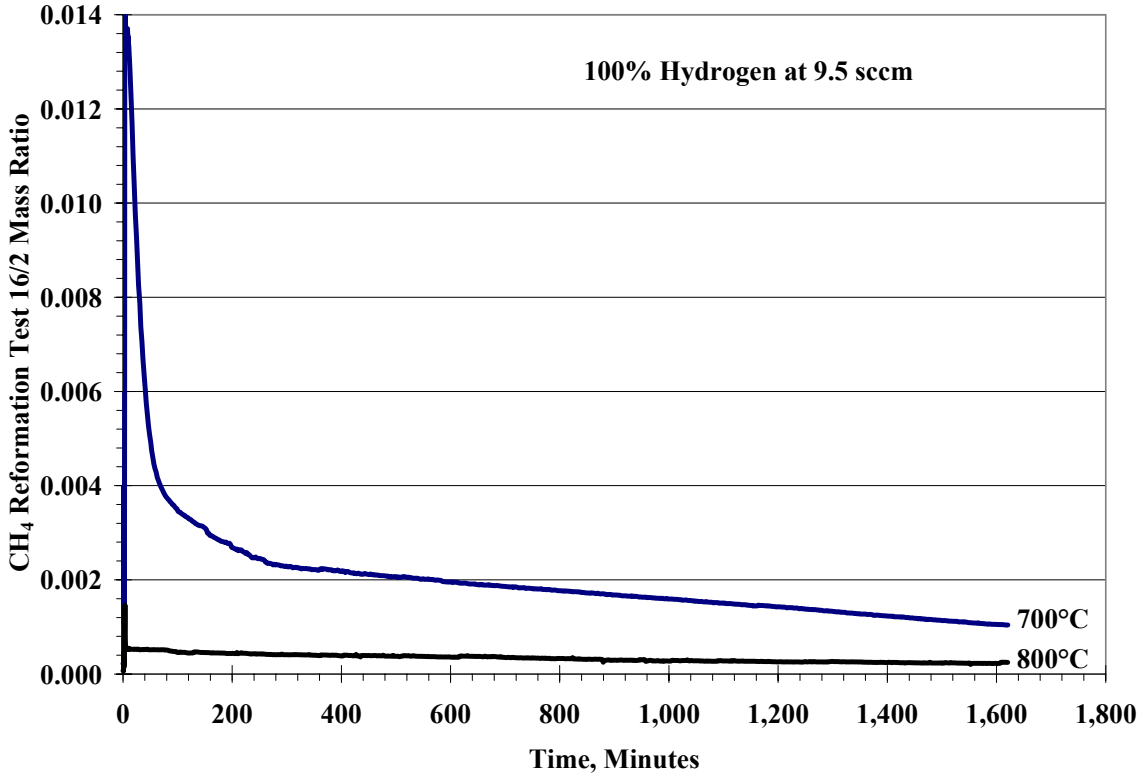

Figure 15. Post-Methane Cracking Test Methane Reformation

Figure 17 is similar to Figure 16, but for tests using a hydrogen carrier: only partial pressures large enough to be identified in the figure were labeled. Methane partial pressures for tests with only carbon dioxide in hydrogen were estimated using RGA data from tests where both methane and carbon dioxide in hydrogen were used. The oscillations in the methane data for 2.5% carbon dioxide were caused by variations in the RGA pressure from unknown reasons: possibly from varied performance of the RGA backing vacuum pump. The test with the 2.5%+2.5% mixture at 800°C was terminated at 25.75 hours due to a vacuum pump failure. The test with 5% carbon dioxide feed at 800°C was effectively terminated at 25.3 hours when the inlet pressure to the bed increased to over 2100 torr, which caused the supply flow of carbon dioxide to decrease and then stop completely.

The methane partial pressures in Figures 16 and 17 for 2.5% and 5% methane feed at 700°C were roughly proportional to feed concentration with 5% methane giving slightly higher partial pressures in helium than in hydrogen. Equilibrium calculations for Equation 10 using a hydrogen carrier show both feed compositions would attain the same equilibrium conditions of 10.5% methane and 89.5% hydrogen thus explaining why the methane partial pressures for 2.5% and 5% methane in hydrogen were virtually the same. Having the same equilibrium methane concentration for both feed conditions and having the exit methane partial pressures proportional to the methane feed partial pressure supports the first order mechanism proposed in Equation 12.

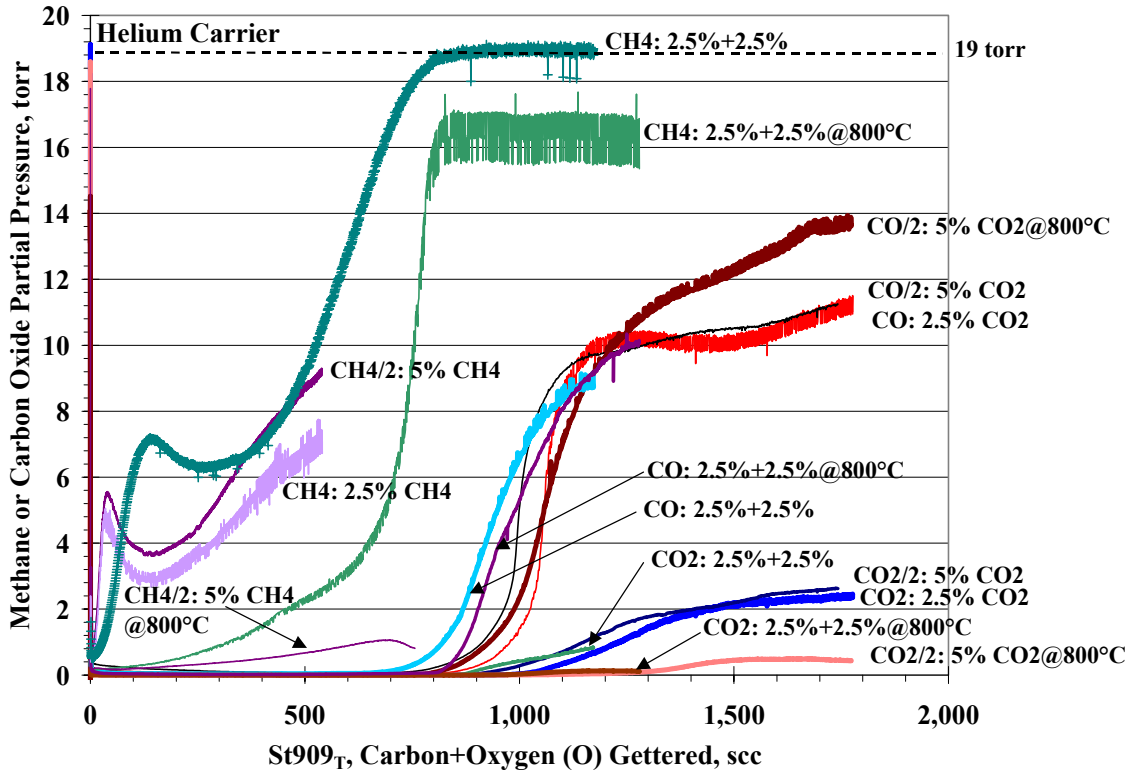

Figure 16. Outlet Gas Partial Pressures in Helium

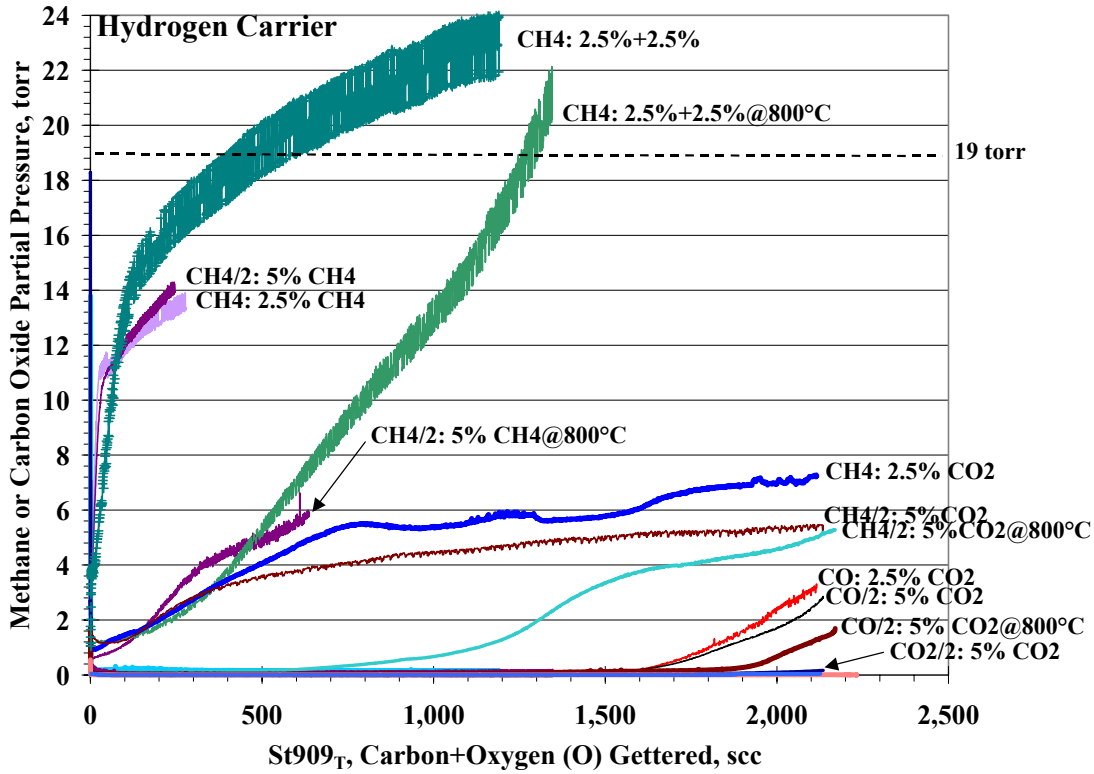

Figure 17. Outlet Gas Partial Pressures in Hydrogen

Carbon Dioxide Cracking

For carbon dioxide in helium, there is little carbon dioxide or carbon monoxide released from the bed in the early part of the tests. As tests proceeded, carbon monoxide was detected before carbon dioxide was detected exiting the bed. The bond strength, or activation energy, to remove one oxygen atom from carbon dioxide is 127 kcal/mole while the energy required to break the second oxygen bond with the carbon is 257 kcal/mole.[9] Based on the large difference in bond strengths, carbon dioxide and carbon monoxide were assumed to be gettered according to the reactions

$$CO_2 + M(surface) \rightarrow CO + MO(surface) \quad (16)$$

$$MO(surface) + M(bulk) \rightarrow M(surface) + MO(bulk) \quad (17)$$

$$CO + 2M(surface) \rightarrow MC(surface) + MO(surface) \quad (18)$$

$$MC(surface) + M(bulk) \rightarrow M(surface) + MC(bulk) \quad (13)$$

$$MO(surface) + M(bulk) \rightarrow M(surface) + MO(bulk) \quad (17)$$

where MO is an unspecified form of oxygen with the metal, possibly dissolved oxygen or a metal oxide.

Another possible explanation for the formation of carbon monoxide is the reverse Bouduard reaction forming carbon monoxide:

$$CO_2 + MC(surface) \rightarrow 2CO + M(surface) \quad (19)$$

Figure 16 shows for 5% carbon dioxide feed at 700°C, the partial pressures for both carbon oxides were twice as large as those for 2.5% carbon dioxide feed at 700°C. The proportionality between the partial pressures of carbon dioxide in the feed and carbon monoxide exiting the reactor would disfavor Equation 19: doubling the feed carbon dioxide partial pressure for Equation 19 would be expected to more than double the amount of carbon monoxide formed. This proportionality supports the reaction mechanisms shown in Equations 16 and 18.

In Figure 16, it appears that when $St909_T$ was between 640 and 840 scc, Equation 16 still occurred at near 100% efficiency, but Equations 17 and 13 were of insufficient rates to complete decomposition of carbon monoxide via Equation 18. As $St909_T$ exceeded 875 scc, the rate of Equation 16 decreased and carbon dioxide was detected exiting the reactor.

When the carbon dioxide cracking test temperature was increased from 700°C to 800°C, the increase in rate of Equation 16 appeared greater than for Equation 17. This explains why in Figure 16, 5% carbon dioxide cracking produced a lower carbon dioxide partial pressure and a corresponding increase in carbon monoxide partial pressure at 800°C compared to 700°C. Constant carbon monoxide plus carbon dioxide exiting the bed further supports Equations 16 and 18 over Equation 19 for carbon monoxide formation and also explains the similar ε_{COX} values

obtained at 700°C and 800°C for 5% carbon dioxide in helium in Figures 3a and 3b, as well as the different ε_{CO2} values seen in Figures 2a and 2b.

Ammonia Cracking

The reduction in ε_M from the addition of ammonia was attributed to nitrogen absorption by and reaction with the getter. The approximately 3% hydrogen created by ammonia cracking did not significantly impact ε_M since ε_M values for 5% methane in 10% hydrogen/85% helium[8] were greater than ε_M values shown in Figure 1b for 5% methane with 2% ammonia in helium.

Ammonia cracking can be represented by the reactions

$$NH_3 + M(surface) \rightarrow MN(surface) + \tfrac{3}{2} H_2 \quad (20)$$

$$MN(surface) + M(bulk) \rightarrow M(surface) + MN(bulk) \quad (21)$$

$$NH_3 + MN(surface) \rightarrow M(surface) + N_2 + \tfrac{3}{2} H_2 \quad (22)$$

where MN is an unspecified form of nitrogen with the metal.

Figure 18 shows select RGA ion currents relative to the mass 84 ion current for tests with the 2.5%+2.5% mixture in helium at 700°C, with and without 2% ammonia in the feed. For the test without ammonia in the feed, the mass 28 signal increased starting approximately halfway through the test. With ammonia in the feed, the mass 28 signal increased at one rate at the start of the test and then transitioned to a greater rate at approximately the same point in the test as for the test without ammonia: a negative off-set of 35 in the 28/84 ratio for the test with ammonia yields a 28/84 plot similar to that obtained for the test without ammonia.

The initially low 28/40 ratio observed in Figure 18 when cracking 5% methane with the 2% ammonia/98% helium carrier gas supports nitrogen decomposing on the getter and diffusing into the bulk: Equations 20 and 21. The increasing and then almost level 28/40 ratio was attributed to a decreased rate of Equation 21 leaving more nitrogen near the surface leading to an increased rate of Equation 22. For the test with 5% carbon dioxide with 2% ammonia in helium, a plot of the 14/84 ratio, an indicator of nitrogen gas formation, was similar to the 28/40 plot for methane with ammonia test further supporting the proposed nitrogen reactions.

Figure 13 shows the difference between measured and gas composition integration mass gains to be approximately 6% higher for methane cracking in nitrogen than in helium or hydrogen which was attributed to nitrogen gettering via Equation 21. The ε_M plots in Figure 1a having similar slopes for 5% methane and 5% methane plus 2% ammonia in helium was interpreted as MN formed by the getter effectively reducing the amount of M available to remove carbon from the surface to the bulk, Equation 13, which produced a reduced rate of methane cracking via Equation 12. The same interpretation was applied to the ε_M plots in Figure 8 where the ε_M plot slopes without and with nitrogen were similar, but reduced in the presence of nitrogen from ammonia.

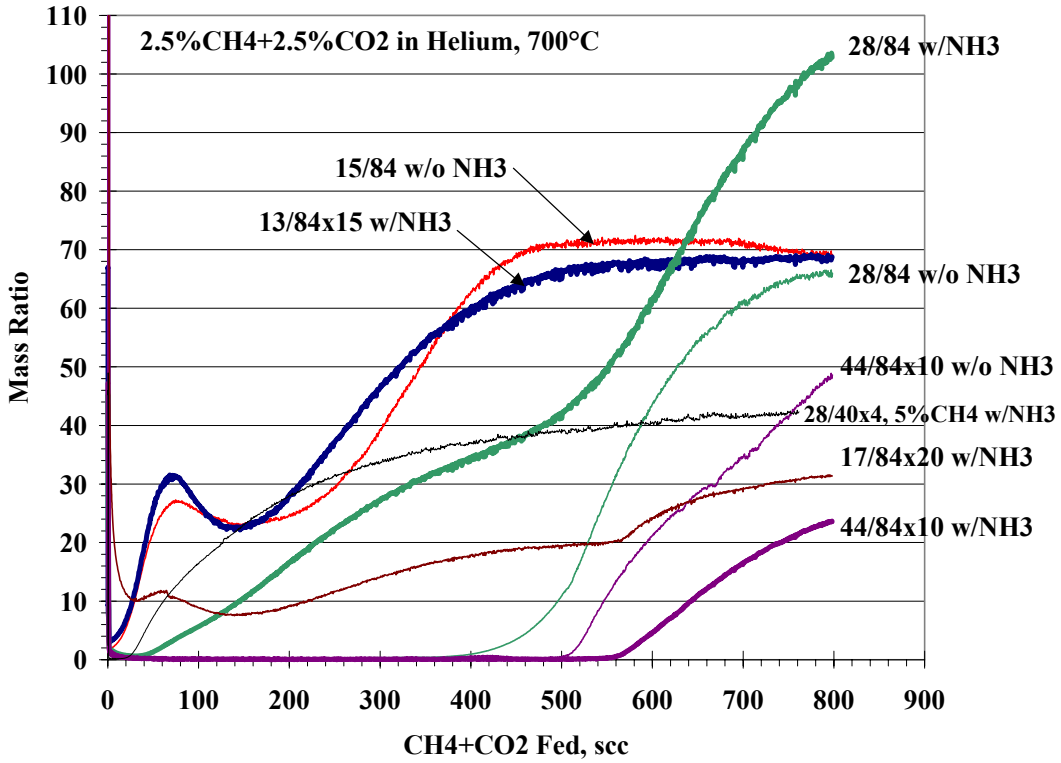

Figure 18. Mass Ratios for Tests with and Without Ammonia

Methane and Carbon Dioxide Cracking

Figure 16 shows when $St909_T$ was approximately 640 scc, methane decomposition with carbon dioxide in the feed was drastically reduced at 800°C and the first rise in carbon monoxide partial pressures can be seen in the figure. With $St909_T$ between 640 and 840 scc, the carbon monoxide partial pressure increased significantly. When $St909_T$ is about 875 scc, the first rise in carbon dioxide partial pressure can be seen in the figure.

Higher methane outlet partial pressures in tests with carbon dioxide in the feed were attributed to each carbon dioxide molecule being cracked occupying three surface metal sites, Equations 16 and 18, reducing the rate of Equation 12. Carbon and oxygen were still being removed from the surface according to Equations 13 and 17, by evidence of no carbon oxides being seen below 640 scc in Figure 16. This indicates complete incorporation of carbon dioxide into the bulk was favored over methane cracking. This is consistent with methane partial pressures at 700°C being high when carbon dioxide was present at given $St909_T$ values (see Figure 17).

Figure 16 shows the initial shape of the methane partial pressure plot at 700°C was altered due to carbon dioxide being cracked: the shift to higher $St909_T$ values for the initial maximum and minimum due to higher getter loading from the carbon dioxide. The roughly same (scaled) partial pressure for 5% methane feed as for the 2.5%+2.5% mixture at $St909_T$ of 535 scc was believed to be coincidental and running a 5% methane only test longer is not expected to give the same methane partial pressure at larger $St909_T$ values.

At 700°C, carbon monoxide incorporation was reduced as $St909_T$ approached 640 scc and the carbon monoxide partial pressure began to rise in Figure 16. At $St909_T$ of approximately 875 scc, methane decomposition essentially stopped, the carbon monoxide partial pressure increased rapidly, and the carbon dioxide partial pressure began to increase. At this $St909_T$ value, it is believed the rate of Equation 13 was greatly reduced which reduced the rates of Equations 17 and 18, which subsequently reduced the rate of Equation 16. That is, as the bulk becomes saturated with carbon and oxygen, surface sites are not available for cracking gas phase species: the most favorable reactions shuts-down last (Equation 16).

Figure 16 shows 5% methane cracking at 800°C had a relatively low (scaled) partial pressure, but when 2.5% carbon dioxide was fed with 2.5% methane, the methane partial pressure was higher at the same $St909_T$ loading without carbon dioxide. For 5% carbon dioxide at 800°C, the carbon monoxide partial pressure begins to rise in Figure 16 at $St909_T$ of approximately 800 scc which was where the methane partial pressure leveled-off at approximately 87% of the feed partial pressure. The carbon dioxide partial pressure was not detected until $St909_T$ of 970 scc and remained very low. Increased rates of carbon and oxygen removal to the bulk (Equations 13 and 17) at 800°C allowed methane decomposition (Equation 12) to proceed at a non-zero rate and allowed more impurities to be gettered into the bulk before carbon oxide partial pressures became apparent.

Methane and Water Formation

Methane was formed in all tests that contained carbon dioxide feed in a hydrogen carrier as shown in Figure 17. Similar results were found when cracking 1% carbon dioxide in a hydrogen carrier with uranium at 500°C.[10] For the 2.5%+2.5% feed at 700°C, there was essentially no net mass gain from methane cracking: a 9 scc loss out of 392 scc methane fed. At 800°C, there was a net 193 scc of methane cracked.

Catalytic methanation reactions, the formation of methane from carbon oxides, are written as

$$CO_2 + 4H_2 \rightarrow CH_4 + 2H_2O \quad (23)$$

$$CO + 3H_2 \rightarrow CH_4 + H_2O \quad (24)$$

A reaction mechanism with the getter can be postulated where methane is formed, but water is not produced:

$$CO_2 + M(surface) \rightarrow CO + MO(surface) \quad (16)$$

$$CO + 2M(surface) \rightarrow MC(surface) + MO(surface) \quad (18)$$

$$MC(surface) + 2H_2 \rightarrow CH_4 + M(surface) \quad (14)$$

Water can be formed by a separate hydrogen reduction reaction:

$$MO(surface) + H_2 \rightarrow M(surface) + H_2O \quad (25)$$

The catalytic reverse shift (reverse of the water-gas shift reaction) is another mechanism for water formation and is written as

$$CO_2 + H_2 \rightarrow CO + H_2O \quad (26)$$

The dominant reaction mechanisms proposed with the getter are Equations 16 and 25.

For the 2.5%+2.5% mixture, Figure 17 shows some methane was cracked at the start of the tests (Equation 12). At 700°C, it was not clear to what extent carbon was removed from the surface (Equation 13), but at 800°C, significantly lower initial methane partial pressures were observed indicating the rate of Equation 13 increased. It is not clear from the Figure 17 data if a constant methane partial pressure at 800°C would be obtained and if it would be lower than that the (potentially constant final) methane partial pressure at 700°C, as was found in Figure 16 for helium, due to a non-zero rate of Equation 13.

The reduced rate of methane cracking in a hydrogen carrier (Equation 14) and the previously described mechanism for the reduced rate of methane cracking with carbon dioxide in helium are combined when cracking methane and carbon dioxide in hydrogen. Methane reformation is the dominant reaction when surface carbon and gas phase hydrogen are relatively abundant. In a hydrogen carrier, the carbon on the surface shown from carbon monoxide cracking (Equation 18) is available for methane formation. If the getter retained no carbon, the maximum methane partial pressure obtainable would be approximately 38 torr: one-half from methane fed and one-half from the carbon dioxide fed.

Figure 17 shows the scaled methane partial pressures for 2.5% and 5% carbon dioxide in hydrogen were similar. This was consistent with the weight gain observed under these conditions. Lower initial methane partial pressure at 800°C compared to 700°C was attributed to a faster rate of Equation 13 at higher temperatures making less carbon available on the surface for methane reformation. As more oxygen was accumulated by the getter at 800°C, the rate of Equation 13 was reduced and more carbon was available at the surface to form methane.

It was once thought that many tests with carbon dioxide and a source of hydrogen from methane cracking, ammonia cracking, or the hydrogen carrier, formed small quantities of water and oxygen as indicated by increased mass 18 and 32 signals near the end of the tests. In some nitrogen carrier tests, increased mass 46 signal near the end of the tests were interpreted as nitrogen oxide compounds, such as nitrogen dioxide (NO_2), being formed. Further analyses showed in most cases, the increased mass 18 and 32 signals were from decreased cracking efficiencies near the end of a test of water and oxygen impurities in the carbon dioxide. The mass 46 signal was attributed to the carbon dioxide isotope $C^{12}O^{16}O^{18}$ that is approximately three orders of magnitude less abundant than the predominant mass 44 isotope, $C^{12}O^{16}O^{16}$.

Water (mass 18) formation was determined by comparing the 18/84 mass ratio obtained at the end of the test to the ratio obtained from post-test analysis of the feed gas (bed bypassing). Figure 19 shows the 18/84 mass ratio for tests where water formation was detected and for one test with an increasing 18/84 mass ratio due to the decreased water cracking efficiency of feed gas impurities. Water formation was not detected for tests at 800°C, for tests with the

2.5%+2.5% mixture in helium or hydrogen, 5% carbon dioxide in 2% ammonia/98% helium, or tests without a source of both hydrogen and oxygen.
Figure 19 shows the 18/84 ratio 2.5% and 5% carbon dioxide in hydrogen at 700°C were similar. The water formation was proportional to the feed carbon dioxide partial pressure; 5% carbon dioxide produced twice as much water (and had twice as much krypton) as 2.5% carbon dioxide feed. The mechanism assumes carbon and oxygen were deposited on the surface by Equations 16 and 18, followed by methane reformation. However, tests with only carbon dioxide had the highest oxygen loading of the getter, which eventually reduced the rate of Equation 17 allowing the rate of Equation 25 to become significant. The absence of water formation at 800°C was attributed to Equation 17 removing oxygen from the surface faster than at 700°C which suppressed the rate of Equation 25. It is speculated that if tests with 2.5% methane plus 2.5% carbon dioxide in helium or hydrogen were run longer, water would be formed as the amount of oxygen on the surface increased: this would also be predicted for tests run longer at 800°C.

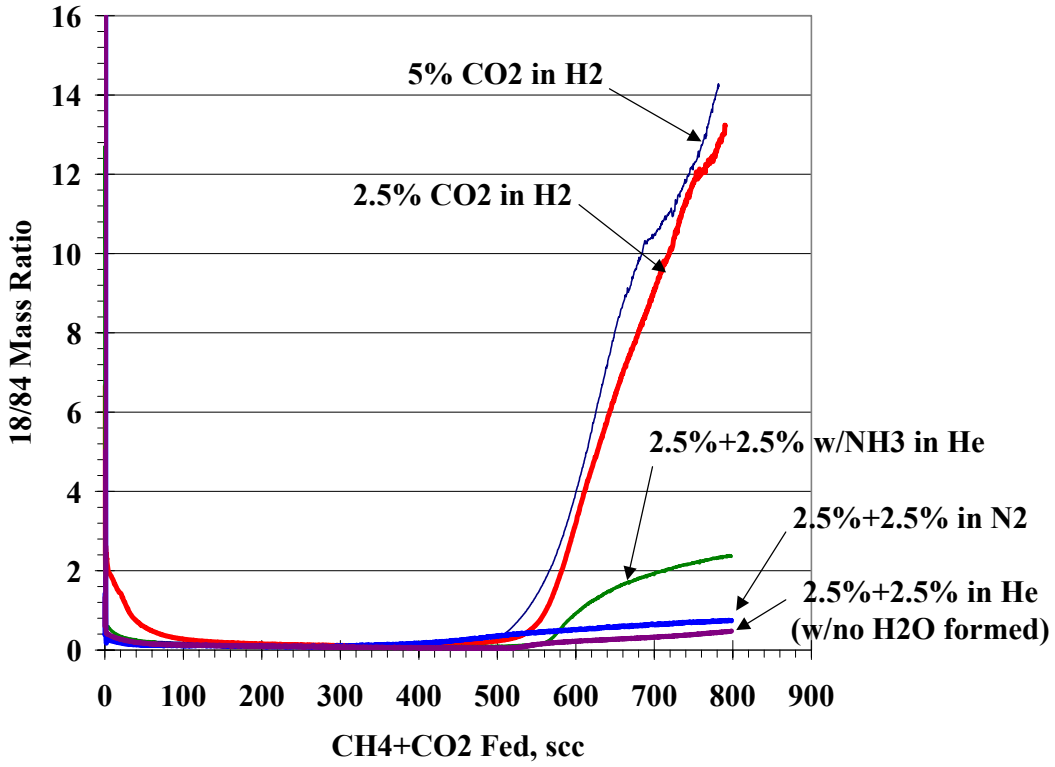

Figure 19. Water Formation Results

Water formation with the 2.5%+2.5% feed mixture with a 2% ammonia/98% helium carrier and for a nitrogen carrier were interpreted as the nitrogen from ammonia cracking or the carrier gas reducing the rate of oxygen removal from the surface via Equation 17 thus increasing the supply of oxygen on the surface which increased the rate of Equation 25. The lack of water formation for 5% carbon dioxide in a 2% ammonia/98% helium carrier was attributed to the greatly reduced rate of Equation 16 carbon dioxide cracking in nitrogen, as shown in Figure 9, which reduced the rate of Equation 18 and the supply of oxygen on the surface available for water formation.

Figure 13 shows good agreement between the measured mass change and the mass change calculated by composition integration for helium and hydrogen carrier gases. The relatively large mass differences for only methane in a nitrogen carrier were interpreted as nitrogen absorption by the St909, which appeared to be relatively independent on the duration of the test, the methane concentration, and temperature. The relatively small mass differences for only carbon dioxide in a nitrogen carrier were interpreted as little absorption of nitrogen by the St909, while a mixture of methane and carbon dioxide yield nitrogen absorptions between the two extremes. Although there was little net absorption of nitrogen with carbon dioxide, there was still an impact of nitrogen on carbon dioxide cracking and water formation. The 0.8% to 1.9% errors for carbon dioxide in hydrogen carrier tests could be attributed to errors in calculating methane production along with errors associated with water formation at 700°C.

The pellet weight change profiles shown in Figures 10, 11, and 12 are what would be expected for a fixed bed reactor: the inlet pellets having a higher weight gain due to their exposure to richer concentrations of the feed impurities. Inlet pellets with mass gains lower than the maximum pellet weight change were attributed to lower inlet temperatures due to variations in applying insulation to the beds between tests.

Table 1 shows the relative volume change for the Zr, Mn, and Fe elements that make up the St909. The carbon alloys can cause a volume change on the order of 10% while the oxides can produce volume changes of 50 to 130%. This is consistent with Figure 14 showing a larger diameter change versus weight change which is mostly attributed to oxygen gettering by the St909 and its subsequent mass and volume change.

Table 1. Volume Change for Selected Alloys

Metal	ρ, g/cc	Alloy	ρ, g/cc	% Vol. Change	Alloy	ρ, g/cc	% Vol. Change	Alloy	ρ, g/cc	% Vol. Change
Zr	6.49	ZrC	6.73	9.1	ZrN	7.09	5.6	ZrO_2	5.89	48.8
Mn	7.20	Mn_3C	6.89	12.1				Mn_2O_3	4.50	129.9
Fe	7.86	Fe_3C	7.694	9.5	Fe_2N	6.35	39.3	Fe_2O_3	5.24	114.5

CONCLUSIONS

St909 can crack methane, carbon dioxide, and ammonia under a variety of operation conditions with efficiencies influenced greatly by other impurities in the gas stream and the carrier gas composition. These bench scale tests, at the relatively high feed impurity levels of 5%, demonstrated the impact of different parameters in relatively short duration tests. Temperature gradients from use of the single zone heater were found to alter the bed gettering profile of St909. The magnitude of these temperature gradients can be reduced by use of a three-zone heater, especially for larger getter beds.

St909 methane cracking increased with increased temperature, but was reduced when the carrier gas was either hydrogen or nitrogen. Hydrogen reversibly suppressed the decomposition of

carbon on the surface of the getter while nitrogen absorption by the getter interfered and reduced the rate of methane decomposition. Switching from cracking methane in a helium carrier gas to flowing hydrogen over the getter made, or reformed, methane. Methane reformation was greater at 700°C than at 800°C due to the higher concentration of carbon on and near the surface of the getter (diffusion of carbon into the bulk was faster at 800°C).

ε_M was reduced when ammonia or carbon dioxide was included in the feed. ε_A was greater than or equal to 97% for all tests and its formation was not detected when methane was cracked in a nitrogen carrier gas. Ammonia cracking initially resulted in nitrogen absorption by the St909 followed by release of nitrogen gas. The interference in methane cracking from ammonia cracking was due to the presence of surface nitrogen and not from the increased hydrogen concentration in the gas phase.

ε_M was also reduced when carbon dioxide was included in the feed. In helium, carbon dioxide decomposition was more facial and inhibited the methane decomposition. Methane cracking in a hydrogen carrier gas was reduced by both the reformation reaction, and the decomposition of the carbon dioxide. Depending on the temperature and the total getter impurity loading, more methane can exit the reactor than entered the reactor, as the carbon from carbon dioxide is converted to methane.

St909 ε_{CO2} values were greater than or equal to 86% for tests with a hydrogen, helium, or helium with 2% ammonia carrier gas. The data support the mechanism where carbon dioxide first loses an oxygen atom to form carbon monoxide which is then decomposed by the getter. Carbon monoxide is seen exiting the reactor before carbon dioxide and the release of these gases occur over distinctly different ranges of total getter loadings.

Cracking carbon dioxide in a hydrogen carrier produced methane throughout the test. In the later stages of the test, water was detected, followed by carbon monoxide. Tests with carbon dioxide in hydrogen also produced the largest pellet weight changes, and fractured the most pellets. In the test at 800°C with 5% carbon dioxide feed, the O.D. of the test bed swelled by 0.010 inches when the pellet originally occupied only 61% of the I.D. of the test bed.

Changes in test conditions that improved carbon dioxide cracking often produced a corresponding increase in carbon monoxide exiting the bed: e.g. the addition of ammonia in the helium carrier gas. At the same total impurity loadings, a bed cracking carbon dioxide in helium produced more carbon monoxide at 800°C than at 700°C.

The inability to quantifiably differentiate nitrogen from carbon monoxide complicated drawing definite conclusions about the quantity of carbon monoxide produced during tests with a nitrogen carrier. Many aspects about the impact of nitrogen on St909 cracking were learned by including ammonia in the test feed mixture and these effects were amplified when using a nitrogen carrier gas. False conjectures about nitrogen oxide formation illustrate some of the difficulties encountered when using an RGA to identify a chemical or fragmentation species by tracking a single ion mass and stress the need for careful data interpretation and/or the need for full mass spectrometer gas analyses to quantify the effects of nitrogen on St909 carbon dioxide and/or carbon monoxide cracking.

REFERENCES

1. C. Boffito, A. Conte, and G. Gasparini, "A New Zr-Based Alloy For Tritium Recovery From Tritiated Water," Trans. Fusion Technol., 27, pp. 69-74 (1995).

2. F. Ghezzi and C. Boffito, "Pressure-Concentration-Temperature Characterization of St909 Getter Alloy With Hydrogen," Vacuum, 47 (6-8), pp. 991-995 (1996).

3. D. H. Meikrantz, J. D. Baker, G. L. Bourne, R. J. Pawelko, R. A. Anderl, D. G. Tuggle, and H. R. Maltrud, "Tritium Process Applications Using SAES Getters for Purification and Collection From Inert Gas Streams," Trans. Fusion Technol., 27, pp. 14-18 (1995).

4. J. D. Baker, D. H. Meikrantz, R. J. Pawelko, R. A. Anderl, and D. G. Tuggle, "Tritium Purification Via Zirconium-Manganese-Iron Alloy Getter ST 909 In Flow Processes," Trans. Fusion Technol., 27, pp. 8-12 (1995).

5. J. D. Baker, D. H. Meikrantz, R. J. Pawelko, R. A. Anderl, and D. G. Tuggle. "Tritium Purification via Zirconium-Manganese-Iron Alloy Getter St909 in Flow Processes". J. Vac. Sci. Technol. A 12(2), Mar/Apr. pp. 548-553 (1994).

6. P. Schira and E. Hutter. "Tritium Cleanup On Hot Uranium Powder". Fusion Technol., 14, pp. 608-613, (1988).

7. R. D. Penzhorn, U. Berndt, E. Kirste, and J. Chabot. "Performance Tests of Palladium/Silver Permeators with Tritium at the Tritium Laboratory Karlsruhe". Fusion Technol., 32, pp. 232-245 (1997).

8. J. E. Klein. "SAES® St909 Bench Scale Methane Cracking Tests". Fusion Sci. & Technol., 41, pp. 998-1003 (2002).

9. R. C. Weast, editor, *CRC Handbook of Chemistry and Physics, 55th Ed.*, CRC Press, Inc., Cleveland, OH (1974-1975).

10. U. Tamm, E. Hutter, G. Neffe, and P. Schira, "Uranium Getters for Tritium Cleanup at the Tritium Laboratory Karlsruhe (TLK)", Fusion Technol., 21, pp. 983-987 (1992).

11. Leybold Inficon Transpector® Gas Analysis System User Guide, Leybold Vacuum Products Inc.

APPENDIX A: RGA EQUATIONS

The partial pressure of species "a" measuring mass "b", PP_a, is written as

$$PP_a = \frac{A_{a,b}}{FF_{a,b}\, XF_a} I_{a,b} \tag{A1}$$

where $FF_{a,b}$ is the fragmentation factor of species a at mass b, XF_a is the ionization probability of substance a relative to nitrogen, $A_{a,b}$ is the analyzer (specific) factor, and $I_{a,b}$ the ion current of species a at mass b. $FF_{a,b}$ and XF_a are species dependent and tabulated values available in RGA and mass spectrometer reference guides. For example, RGA analysis of carbon dioxide yields fragmentation factors of 0.70 for mass 44, 0.11 for mass 28 (carbon monoxide), 0.06 for mass 16 (atomic oxygen), and 0.01 for mass 12 (carbon).[11]

The CO_{out}-to-$CO_{2,in}$ ratio in Equation 4 needs to be determined to calculate ε_{COX}. CO_{out} can be calculated by measuring the ion current at mass 28 and adjusting for the contribution from carbon dioxide fragmentation and nitrogen:

$$I_{CO,28} = I_{ALL,28} - I_{N2,28} - I_{CO2,28} \tag{A2}$$

where the total ion current signal at mass 28 ($I_{ALL,28}$) is the sum of the signals generated by carbon monoxide, nitrogen, and carbon dioxide fragmentation.

Using the definition of carbon dioxide partial pressure:

$$PP_{CO2} = \frac{A_{CO2,44}}{FF_{CO2,44}\, XF_{CO2}} I_{CO2,44} = \frac{A_{CO2,28}}{FF_{CO2,28}\, XF_{CO2}} I_{CO2,28} \tag{A3}$$

and by solving for the analyzer factors in terms of the measured ion currents for the inlet gas

$$I_{CO2,28} = \left(\frac{I_{CO2,28}}{I_{CO2,44}} \right)_{in} I_{CO2,44} \tag{A4}$$

the ion current at mass 28 attributed to carbon dioxide fragmentation can be determined using the ion current of carbon dioxide at mass 44.

The partial pressure of carbon monoxide is given by

$$PP_{CO} = \frac{A_{CO,28}}{FF_{CO,28}\, XF_{CO}} I_{CO,28} \tag{A5}$$

and it is desirable to calculate this quantity without using analyzer factors. The CO_{out}-to-$CO_{2,in}$ ratio in ε_{COX}

$$\frac{CO_{out}}{CO2_{in}} = \frac{PP_{CO,out}}{PP_{CO2,in}} = \frac{\frac{A_{CO,28}}{FF_{CO,28}\ XF_{CO}} I_{CO,28}}{\frac{A_{CO2,44}}{FF_{CO2,44}\ XF_{CO2}} I_{CO2,44,in}} \tag{A6}$$

can be simplified if the analyzer factor for mass 28 is the same for carbon monoxide for carbon dioxide ($A_{CO,28}$ equals $A_{CO2,28}$) and no carbon monoxide or nitrogen are in the feed:

$$\frac{CO_{out}}{CO2_{in}} = \frac{FF_{CO2,28} XF_{CO2}}{FF_{CO,28}\ XF_{CO}} \left[\frac{I_{ALL,28}}{I_{CO2,28,in}} - \frac{I_{CO2,44}}{I_{CO2,44,in}} \right] \tag{A7}$$

Thus, the carbon oxide efficiency can be written as

$$\varepsilon_{COX} = \varepsilon_{CO2} - \frac{FF_{CO2,28} XF_{CO2}}{FF_{CO,28}\ XF_{CO}} \left[\frac{I_{ALL,28}}{I_{CO2,28,in}} - \frac{I_{CO2,44}}{I_{CO2,44,in}} \right] \tag{A8}$$

The difference between ε_{CO2} and ε_{COX} gives a measure of the amount of atomic oxygen gettered. The total amount of oxygen gettered, $St909_O$, is calculated using

$$St909_O = \int_0^t 2 * F_{CO2,in} \left(\varepsilon_{CO2} - \frac{1}{2} \frac{FF_{CO2,28} XF_{CO2}}{FF_{CO,28}\ XF_{CO}} \left[\frac{I_{ALL,28}}{I_{CO2,28,feed}} - \frac{I_{CO2,44}}{I_{CO2,44,feed}} \right] \right) dt \tag{A9}$$